Article

Cell

Impaired Amino Acid Transport at the Blood Brain Barrier Is a Cause of Autism Spectrum Disorder

Graphical Abstract

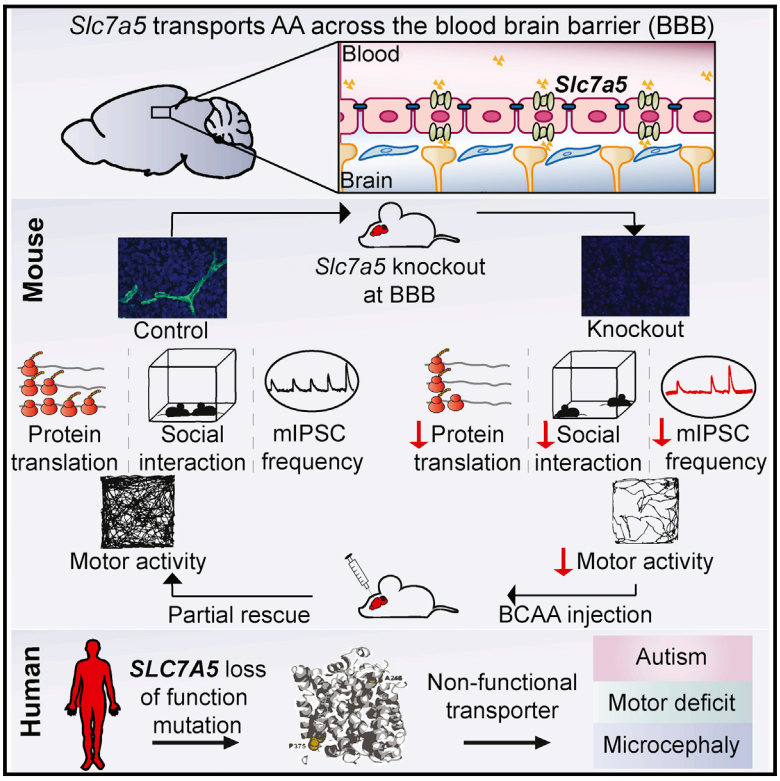

Highlights

- *Slc7a5* is critical for maintaining normal brain BCAA levels
- Brain BCAA deficiency triggers neurobehavioral alterations in mice
- Patients with *SLC7A5* mutations have ASD and motor delay
- *Slc7a5* mutant mouse behavior is partially corrected by BCAA injections

Authors

Dora C. Tărlungeanu, Elena Deliu, Christoph P. Dotter, ..., Murat Gunel, Joseph G. Gleeson, Gaia Novarino

Correspondence

gnovarino@ist.ac.at

In Brief

Mutations in a solute carrier protein that blunts the transport of branched-chain amino acids lead to neurological and behavioral abnormalities associated with autism spectrum disorder.

Data Resources

GSE87808
GSE39447

Tărlungeanu et al., 2016, Cell *167*, 1481–1494
December 1, 2016 © 2016 Elsevier Inc.
http://dx.doi.org/10.1016/j.cell.2016.11.013

CellPress

Article

Cell

Impaired Amino Acid Transport at the Blood Brain Barrier Is a Cause of Autism Spectrum Disorder

Dora C. Tărlungeanu,[1] Elena Deliu,[1] Christoph P. Dotter,[1] Majdi Kara,[2] Philipp Christoph Janiesch,[3] Mariafrancesca Scalise,[4] Michele Galluccio,[4] Mateja Tesulov,[1] Emanuela Morelli,[1] Fatma Mujgan Sonmez,[5] Kaya Bilguvar,[6,7] Ryuichi Ohgaki,[8] Yoshikatsu Kanai,[8] Anide Johansen,[9] Seham Esharif,[2] Tawfeg Ben-Omran,[10] Meral Topcu,[11] Avner Schlessinger,[12] Cesare Indiveri,[4] Kent E. Duncan,[3] Ahmet Okay Caglayan,[13,14] Murat Gunel,[14] Joseph G. Gleeson,[9] and Gaia Novarino[1,15,*]

[1]Institute of Science and Technology (IST) Austria, Klosterneuburg 3400, Austria
[2]Department of Pediatrics, Tripoli Children's Hospital, Tripoli, Libya
[3]Center for Molecular Neurobiology (ZMNH), University Medical Center Hamburg-Eppendorf (UKE), Hamburg 20251, Germany
[4]Department DiBEST, Unit of Biochemistry & Molecular Biotechnology, University of Calabria, Arcavacata di Rende, Italy
[5]Association of Developmental Child Neurology, Ankara, Turkey
[6]Department of Genetics, Yale School of Medicine, New Haven, CT 06510, USA
[7]Yale Center for Genome Analysis, Yale School of Medicine, Orange, CT 06477, USA
[8]Department of Bio-system Pharmacology, Graduate School of Medicine, Osaka University, Osaka Prefecture 565-0871, Japan
[9]Department of Neuroscience, UCSD, Investigator, Howard Hughes Medical Institute, Rady Children's Institute for Genomic Medicine, San Diego, CA 92093, USA
[10]Section of Clinical and Metabolic Genetics, Department of Pediatrics, Hamad Medical Corporation, Doha, Qatar
[11]Department of Pediatric Neurology, Hacettepe University Children's Hospital, Ankara, Turkey
[12]Department of Pharmacological Sciences, Icahn School of Medicine at Mount Sinai, New York, NY 10029, USA
[13]Department of Medical Genetics, School of Medicine, Istanbul Bilim University, Istanbul, Turkey
[14]Departments of Neurosurgery, Genetics, and Neurobiology, Program in Brain Tumor Research, Yale Program on Neurogenetics and Yale Comprehensive Cancer Center, Yale School of Medicine, New Haven, CT 06510, USA
[15]Lead Contact
*Correspondence: gnovarino@ist.ac.at
http://dx.doi.org/10.1016/j.cell.2016.11.013

SUMMARY

Autism spectrum disorders (ASD) are a group of genetic disorders often overlapping with other neurological conditions. We previously described abnormalities in the branched-chain amino acid (BCAA) catabolic pathway as a cause of ASD. Here, we show that the *solute carrier transporter 7a5* (*SLC7A5*), a large neutral amino acid transporter localized at the blood brain barrier (BBB), has an essential role in maintaining normal levels of brain BCAAs. In mice, deletion of *Slc7a5* from the endothelial cells of the BBB leads to atypical brain amino acid profile, abnormal mRNA translation, and severe neurological abnormalities. Furthermore, we identified several patients with autistic traits and motor delay carrying deleterious homozygous mutations in the *SLC7A5* gene. Finally, we demonstrate that BCAA intracerebroventricular administration ameliorates abnormal behaviors in adult mutant mice. Our data elucidate a neurological syndrome defined by *SLC7A5* mutations and support an essential role for the BCAA in human brain function.

INTRODUCTION

Autism spectrum disorders (ASD) is a group of syndromes of heterogeneous etiologies characterized by impairment in social interactions, verbal communication, and repetitive behaviors. A number of twin and family studies have shown that genetics play a significant role in the development of ASD (Bailey et al., 1995; Folstein and Rutter, 1977). However, the genetic architecture of ASD is very complex and mutations in a single gene rarely account for a significant proportion of ASD patients. Despite their genetic heterogeneity, ASD may be less diverse functionally. Indeed, in many instances the great number of genes implicated in neurological disorders converges on a smaller number of biological pathways (De Rubeis et al., 2014).

We recently identified mutations in the gene *branched chain keto-acid dehydrogenase kinase* (*BCKDK*) in several patients with ASD, intellectual disability (ID), and epilepsy (Novarino et al., 2012). *BCKDK* is the enzyme responsible for the rate-limiting step in the catabolic pathway of the branched-chain amino acids (BCAAs), a group of essential amino acids comprising valine, leucine, and isoleucine. The most direct consequence of *BCKDK* mutations is a hyper-catabolism of the BCAAs, resulting in abnormally low levels of serum and brain BCAAs (Novarino et al., 2012).

The brain is dependent on a constant supply of BCAAs from the periphery. Should BCAAs be substantially important for the brain, factors facilitating BCAA uptake might be critical for the proper function of the CNS. The large neutral amino acid transporter 1 (LAT1) is encoded by the *SLC7A5* gene (Verrey, 2003). The transporter is localized at the blood brain barrier (BBB) and forms a heterodimer with the glycoprotein CD98, encoded by the *SLC3A2* gene.

Here, we studied a mouse model in which *Slc7a5* was deleted from the BBB and found that *Slc7a5* is particularly

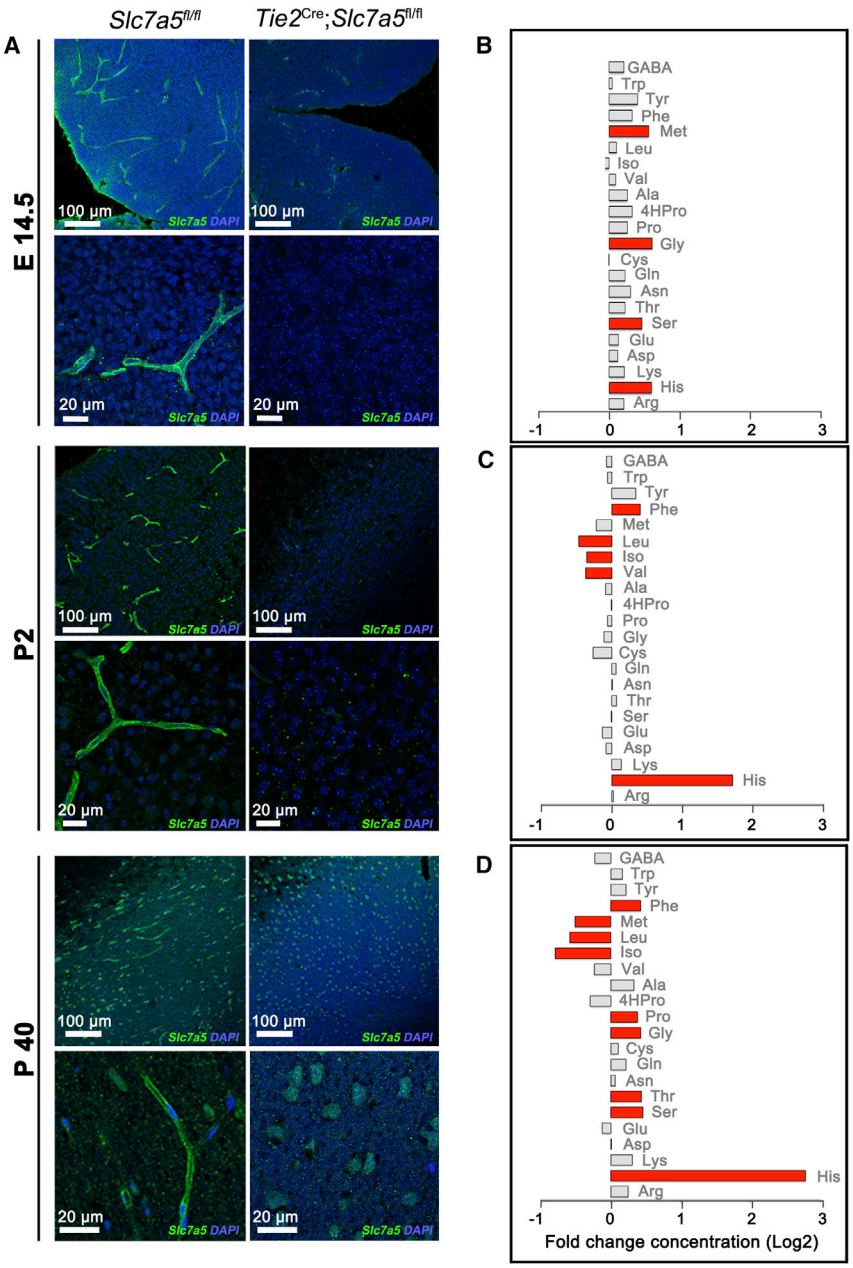

Figure 1. Slc7a5 Mediates BCAA Flux at the BBB

(A) Representative images showing Slc7a5 (green) localization at the BBB in control animals (*Slc7a5*$^{fl/fl}$, left) and its complete deletion in endothelial cells of the BBB in Cre positive mice (*Tie2*^{Cre}*;Slc7a5*$^{fl/fl}$, right). Immunostainings were performed in cortical slices at embryonic day 14.5 (E14.5 top), postnatal day 2 (P2, middle) and adulthood (> P40, bottom). Nuclei were stained with DAPI (blue).

(B–D) Brain amino acid levels in *Tie2*^{Cre}*;Slc7a5*$^{fl/fl}$ mice at E14.5 (B), P2–P14 (C), and >P40 (D). Levels of amino acids were normalized on protein concentration and shown as fold change (log2 transformed) to levels in age-matched controls. In red are represented the amino acids with a fold change >1.3 and p value < 0.05 (n > 4 mice/genotype/time point). See also Figures S1 and S2 and Table S1.

RESULTS

SLC7A5 Mediates BCAA Flux at the BBB

Earlier in vitro studies described the sodium-independent LAT1 as a large neutral amino acid (LNAA) transporter, including the BCAAs (Mastroberardino et al., 1998). The light subunit of the carrier, encoded by *SLC7A5*, is sufficient to transport LNAAs (Napolitano et al., 2015). The contribution of *SLC7A5* to brain LNAA/BCAA homeostasis in vivo, however, remains completely unknown.

To understand the physiological role of *Slc7a5* in vivo, we employed a conditional (floxed) *Slc7a5* knock out mouse line (*Slc7a5*^{fl}) (Sinclair et al., 2013). In wild-type (WT) animals, *Slc7a5* is considerably expressed in the plasma membrane of the endothelial cells of the BBB during development and in adulthood but it is mostly undetectable in other tissues (Figures 1A and S1A–S1C). Thus, we crossed the *Slc7a5*^{fl} mouse with the *Tie2Cre* mouse line, expressing the Cre recombinase starting from embryonic day (E) 11.5 in the endothelial cells of blood vessels and BBB (Figure S1D) (Kisanuki et al., 2001). As expected, endothelial cells of the BBB of *Tie2*-^{Cre}*;Slc7a5*$^{fl/fl}$ mice show complete lack of expression of *Slc7a5* (Figure 1A).

The exchange between blood and cerebrospinal fluid of a wide range of metabolically important molecules, including amino acids, is known to be constrained already at early developmental stages, arising with the BBB formation. However, some studies reported that many amino acids, including the BCAAs, are transported into the developing brain at much higher rate than in adulthood (Braun et al., 1980; Lefauconnier and Trouvé, 1983). Whether this reflects a greater metabolic demand of the

important to set brain BCAA levels within a normal range. Mice with defective BCAA transport at the BBB show abnormal activation of the amino acid response (AAR) pathway and a corresponding reduction in mRNA translation along with neuronal activity imbalance and behavioral problems. To probe whether *SLC7A5* is essential also in humans, we performed genetic analysis of a cohort of neurological pediatric patients. We identified and functionally validated mutations in *SLC7A5* in several patients with ASD and motor coordination problems. Notably, neurological abnormalities can be treated in adult mice by 3-week long intracerebroventricular (i.c.v.) BCAA delivery.

developing brain or the immaturity of the BBB is unknown (Watson et al., 2006). Hence, we asked how removal of *Slc7a5* from the BBB affects brain amino acid levels at different developmental stages.

We found that E14.5 *Tie2*^{Cre}*;Slc7a5*$^{fl/fl}$ mice don't show major changes in brain LNAA and BCAA levels (Figure 1B), suggesting that either at E14.5 the BBB is still immature, with amino acids leaking into the brain, or another transporter may regulate LNAA and BCAA fluxes across the BBB during early development. In contrast, after birth and in adult stages, brain BCAA (especially leucine and isoleucine) levels are abnormally low in *Tie2*^{Cre}*;Slc7a5*$^{fl/fl}$ animals (Figures 1C and 1D), indicating that *Slc7a5* expression is essential to regulate BCAA uptake by the brain. Surprisingly, the brain levels of several other LNAAs (e.g., tyrosine and tryptophan) in *Slc7a5* mutants are comparable to the ranges observed in control (*Tie2*^{Cre}*;Slc7a5*$^{fl/+}$) animals, while a few other amino acids (e.g., histidine, serine, and phenylalanine) show an elevated level in mutants compared to controls. In particular, brain histidine concentration is several fold higher in the *Tie2*^{Cre}*;Slc7a5*$^{fl/fl}$ mice than in control animals (Figures 1B–1D). This result supports the idea that SLC7A5 works as an antiporter, and histidine is the main counter amino acid (Figure S2) (Napolitano et al., 2015).

Thus, in the absence of *Slc7a5* expression at the BBB, the mammalian brain accumulates histidine while failing to gather normal amounts of BCAAs. Importantly, neither the serum amino acid profile nor the level of brain neurotransmitters are affected in the *Tie2*^{Cre}*;Slc7a5*$^{fl/fl}$ animals (Figure S2C; Table S1). While this last result contradicts previous hypotheses (del Amo et al., 2008), it is in agreement with our in vitro experiments showing that SLC7A5 does not facilitate the movement of neurotransmitters (Figures S2A and S2B).

Deletion of *Slc7a5* from the BBB Activates the AAR Signal Transduction Pathway in the Brain

In vitro, SLC7A5 transports not only the BCAAs but also other LNAAs, including phenylalanine, tyrosine, and tryptophan (Napolitano et al., 2015). However, brain levels of these amino acids were not reduced in *Tie2*^{Cre}*;Slc7a5*$^{fl/fl}$ mice but rather slightly increased (Figure 1D). This suggests that additional BBB-located transporters might efficiently compensate for *Slc7a5* loss by mediating the passage of several LNAAs, but not of BCAAs. Indeed, RNA-sequencing (RNA-seq) of mouse brain revealed a significant upregulation of *Slc7a1* and *Slc7a3* genes (Figures 2A and 2B) encoding for the amino acid transporters Cat1 and Cat3 (Fotiadis et al., 2013). This finding suggests that in vivo Cat1 and Cat3 may contribute to preserve brain levels of LNAAs, other than BCAAs, in the *Tie2*^{Cre}*;Slc7a5*$^{fl/fl}$ mice.

Furthermore, differential gene expression analysis revealed the upregulation of genes implicated in serine biosynthesis in *Tie2*^{Cre}*;Slc7a5*$^{fl/fl}$ mice (Figure 2B), explaining the modest but significant increase in brain serine level observed in the mutant animals (Figure 1D). An increase in the expression of genes encoding for amino acid transporters and serine biosynthetic enzymes has been previously linked to the activation of the AAR, a process implemented by individual cells to respond to amino acid deprivation (Kilberg et al., 2009). Consistently, RNA-seq analysis of *Tie2*^{Cre}*;Slc7a5*$^{fl/fl}$ mouse brain revealed the upregulation of a number of other amino acid-related genes (e.g., aminoacyl-tRNA synthetases) (Figures 2A and 2B). Among them, we noticed a significant upregulation of mRNAs encoding for the amino acid responsive transcription factors *Atf4* and *Atf5* and the eukaryotic initiation factor 4E binding protein, *4ebp1* (Figure 2A), all part of the AAR pathway. *Atf4* and *Atf5* have been implicated in the regulation of the CNS development and function. Specifically, *Atf4* modulates synaptic plasticity and long-term memory formation (Chen et al., 2003), while *Atf5* has been implicated in cell growth and development, especially in the nervous system (Angelastro et al., 2003). Aberrant expression of *Atf4* and/or *Atf5* has been implicated in cognitive dysfunctions and neuropsychiatric abnormalities, including altered emotional behavior (Green et al., 2008) and behavioral inflexibility (Trinh et al., 2012).

Importantly, our gene expression analysis did not reveal any abnormality ascribable to increased histidine levels, suggesting that, despite histidine being the most affected amino acid by *Slc7a5* deletion, changes in its level do not lead to severe molecular defects. Similarly, we did not detect changes attributable to alterations of other amino acids such as phenylalanine.

Altered mRNA Translation in *Slc7a5* Mutant Mice

Amino acid deprivation and activated AAR signaling pathway are associated with suppression of protein synthesis via phosphorylation of the translation initiation factor eIF2α. In the past few years, several genes regulating mRNA translation have been implicated in cognitive deficits (Gkogkas et al., 2013; Santini et al., 2013). We therefore examined the effect of *Slc7a5* knock out at the BBB on translation and associated pathways in the brain.

To assess the impact of leucine and isoleucine deficiency on mRNA translation in the brain of *Tie2*^{Cre}*;Slc7a5*$^{fl/fl}$ mice, we first performed western blot analysis of neocortical lysates obtained from wild-type and mutant animals. Specifically, we evaluated the expression and activity status of a number of proteins involved in the regulation of protein synthesis (Figure 2C). We observed a significant increase in the total levels of 4EBP1 protein (Figure 2C), consistent with increased 4EBP1 mRNA levels seen in our RNA-seq data (Figure 2A) and of phosphorylated eukaryotic initiation factor 2 alpha (eIF2α) (Figure 2C), indicating that removal of *Slc7a5* from the BBB and the consequent decrease in brain BCAA concentration may lead to the suppression of cap-dependent translation initiation. In contrast, in none of our experiments did we detect abnormal activation of the mammalian target of rapamycin (mTOR) pathway (Figure 2C), whose activity was shown to be regulated by leucine levels in vitro (Wolfson et al., 2016). This may suggest that in vivo, under chronic leucine deficiency, the mTOR complex is alternatively regulated.

To test whether abnormal regulation of 4EBP1 and eIF2α in mice lacking *Slc7a5* leads to changes in translation efficiency in the brain, we performed polysome profiling of wild-type and *Tie2*^{Cre}*;Slc7a5*$^{fl/fl}$ cortices. Importantly, in *Tie2*^{Cre}*;Slc7a5*$^{fl/fl}$ mouse cortical lysates, we observed a significant shift of ribosomes from actively translating polysomes toward the monosomal fraction (Figure 2D), the hallmark of decreased translation initiation. We conclude that BCAA shortage and associated effects of 4EBP1 levels and increased eIF2α phosphorylation elicit deficient translation initiation in the brain.

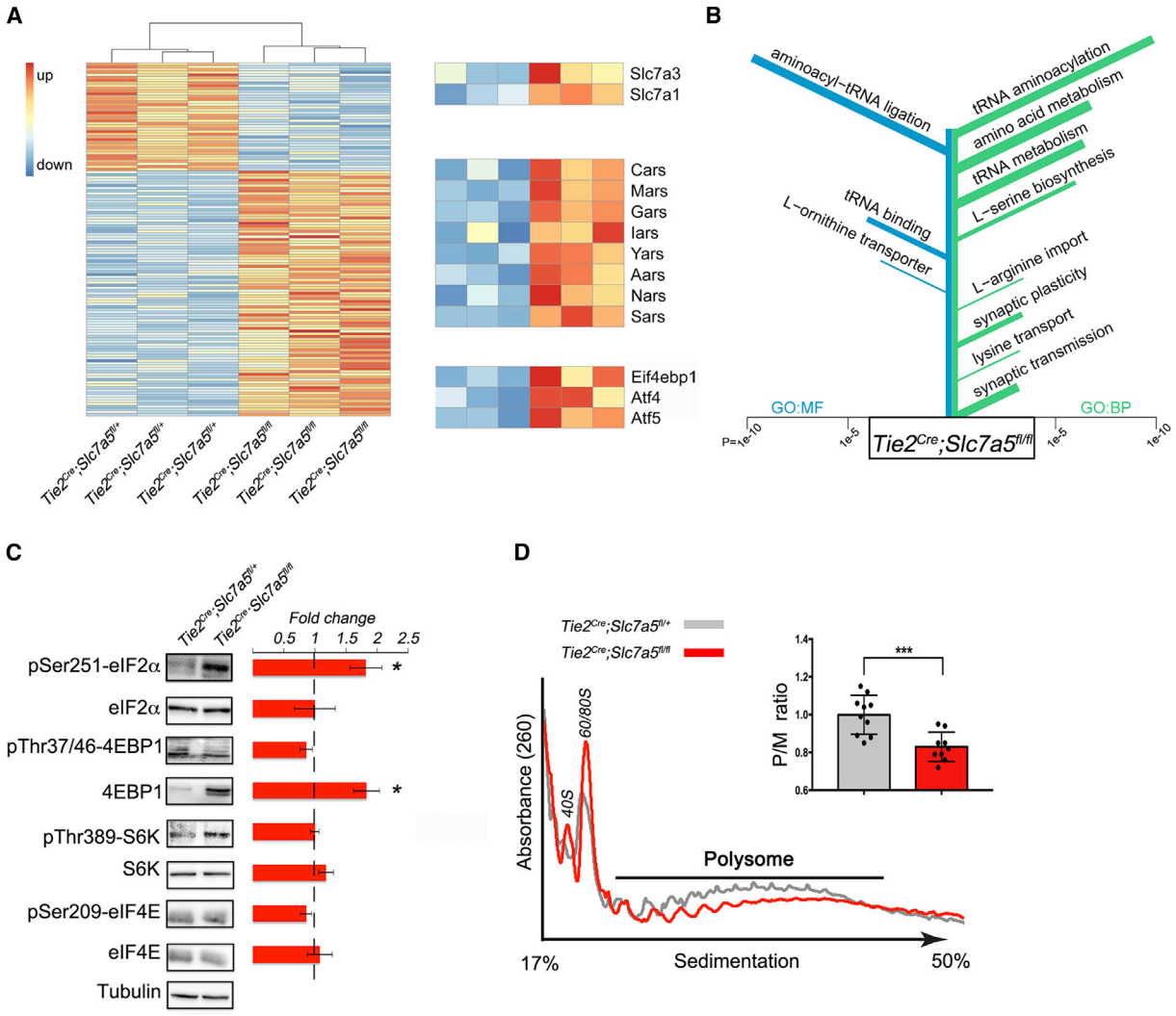

Figure 2. Activation of the Amino Acid Response Pathway in the Brain of *Slc7a5* Mutant Mice

(A) RNA sequencing of adult brain in *Tie2*^{Cre};*Slc7a5*$^{fl/+}$ and *Tie2*^{Cre};*Slc7a5*$^{fl/fl}$ mice revealed 131 differentially expressed genes (FDR-adjusted p value $\leq$ 0.05). The heatmap displays log transformed count data normalized to library size. Genes expressed at lower levels in *Tie2*^{Cre};*Slc7a5*$^{fl/fl}$ (40 genes) are displayed at the top and genes upregulated in *Tie2*^{Cre};*Slc7a5*$^{fl/fl}$ (91 genes) are shown at the bottom. Zoomed rows on the right emphasize differentially expressed genes associated with amino acid import (GO:0089718), tRNA amino acylation (GO:0006418,) and amino acid response, respectively (n = 3 mice/genotype).

(B) Results of GO Enrichment analysis on the set of 131 differentially expressed genes. Terms are sorted according to p value with the most significantly enriched terms at the top: GO terms for molecular functions (GO:MF, left, blue); GO terms for biological processes (GO:BP, right, green). The length of each bar indicates the p value while the width indicates the amount of genes in the set associated with the term.

(C) Western blot analysis from cortical lysates of *Tie2*^{Cre};*Slc7a5*$^{fl/+}$ (control) and *Tie2*^{Cre};*Slc7a5*$^{fl/fl}$ mice, indicating that mutants exhibit increased phospho-eIF2α and total 4EBP1 protein levels but normal levels of total eIF2α, phospho-4EBP1, phospho-S6K, S6K, phospho-eIF4E, and eIF4E. Tubulin was used as internal control. Representative blots (left) and fold change ratio (right); *p < 0.05 (means ± SEM; n $\geq$ 4 mice/genotype).

(D) Polysome profile from cortical lysates of control and *Tie2*^{Cre};*Slc7a5*$^{fl/fl}$ mice. Typical tracings indicating positions of 40S, 60S, and 80S ribosome peaks and polysome (P)/monosome (M) ratio quantifications; ***p < 0.001 (right inset: means ± SEM; n = 10 control and n = 9 mutant mice).

Slc7a5 Conditional Knock Out Animals Show Motor Delay and Autism-Related Phenotypes

Behavioral impairments resulting from abnormal regulation of cap-dependent translation have been previously described (Banko and Klann, 2008; Santini et al., 2013; Trinh et al., 2012). Thus, we tested *Tie2*^{Cre};*Slc7a5*$^{fl/fl}$ mice for global behavioral changes. *Tie2*^{Cre};*Slc7a5*$^{fl/fl}$ mice are born at Mendelian ratio and appear normal in size but display kyphosis (44% of mutant mice) and hind limb clasping (89% of mutant mice). In an open field, *Tie2*^{Cre};*Slc7a5*$^{fl/fl}$ mice show reduced explorative behavior and lower velocity (Figure 3A). Rearing, a form of vertical exploration, was significantly reduced in the *Tie2*^{Cre};*Slc7a5*$^{fl/fl}$ mice (Figure 3B). Nonetheless, *Slc7a5* mutant mice and wild-type littermates have similar habituation time course (Figure S3A), suggesting that the diminished activity results from locomotion defects rather than a faster habituation to the field. Therefore,

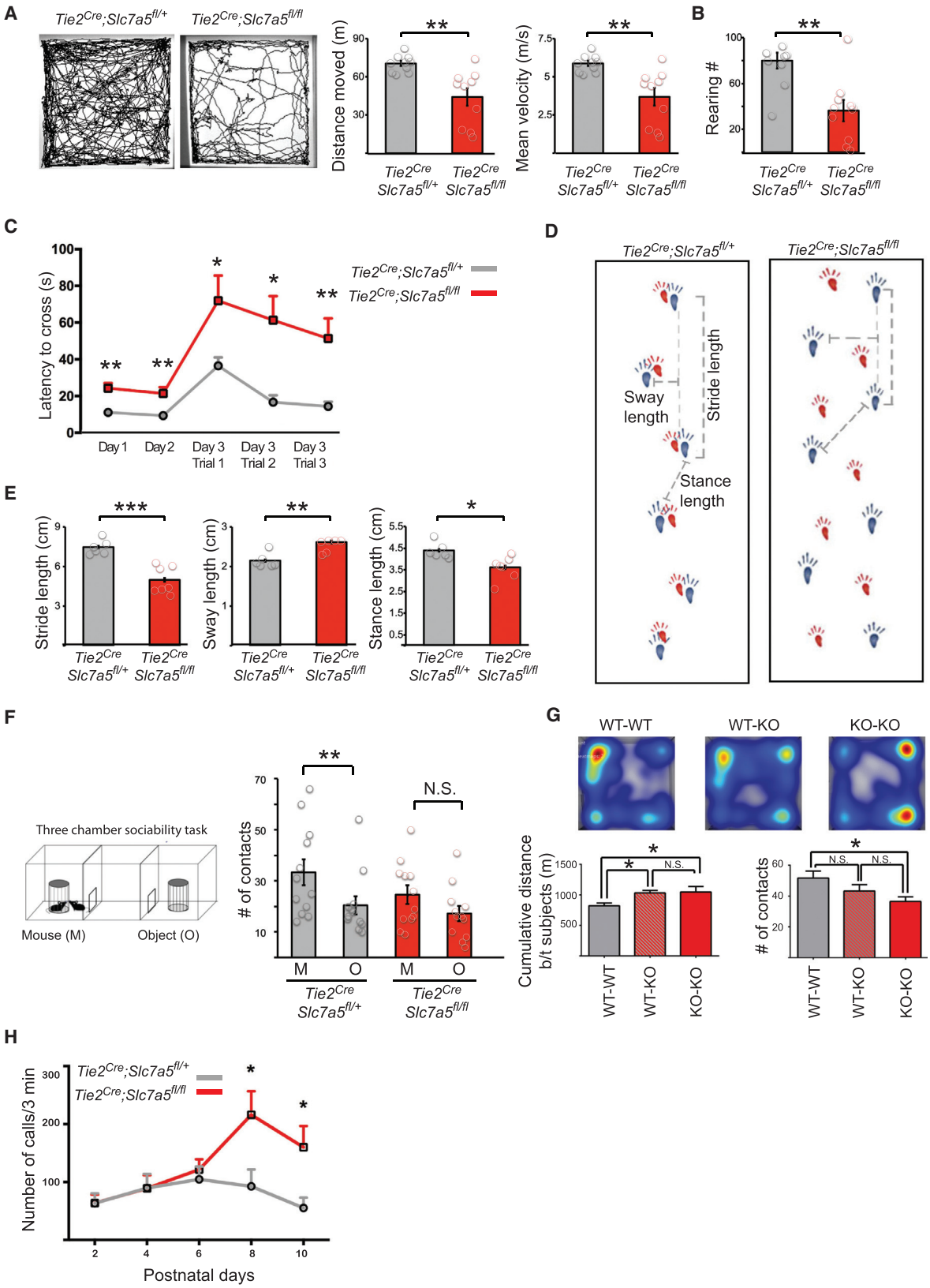

(legend on next page)

we tested the *Tie2*^{Cre};*Slc7a5*$^{fl/fl}$ mice for fine motor coordination and locomotion problems. Indeed, *Tie2*^{Cre};*Slc7a5*$^{fl/fl}$ animals presented significant difficulties in the walking beam test (Figure 3C) and gait abnormalities (Figures 3D and 3E).

Because in our previous work, we implicated BCAA deficiency in ASD (Novarino et al., 2012), we tested *Tie2*^{Cre};*Slc7a5*$^{fl/fl}$ for autism-like phenotypes. *Tie2*^{Cre};*Slc7a5*$^{fl/fl}$ do not show excessive grooming or perseverative behaviors (Figure S3B), activities that can be, however, severely complicated by the presence of motor deficits in the mutants. Thus, we tested *Tie2*^{Cre};*Slc7a5*$^{fl/fl}$ mice for social interaction abnormalities. We first employed a three-chamber social arena to probe the mutant animals for self-initiated interactions with a wild-type unfamiliar mouse. This analysis revealed that while wild-type mice have more close interactions with an unfamiliar mouse than an object, the *Tie2*^{Cre};*Slc7a5*$^{fl/fl}$ mice show no preference between these two (Figure 3F). We then tested juvenile animals for social play and found that *Tie2*^{Cre};*Slc7a5*$^{fl/fl}$ mice tend to stay farther apart from their cage-mate and display a decreased number of nose-to-nose contacts (Figure 3G). Finally, we measured isolation-induced ultrasonic vocalizations (USVs) emitted by mouse pups separated from the mother. *Tie2*^{Cre};*Slc7a5*$^{fl/fl}$ pups display an increased number of USVs starting from P8 when compared with their wild-type littermates (Figure 3H), a behavior observed in other autism models (Gkogkas et al., 2013). Interestingly, the excessive number of USVs emitted by the mutant pups may be due to an increased repetition of a specific repertoire of vocalization patterns (Romano et al., 2013).

Inhibitory Activity Defects in *Tie2*^{Cre};*Slc7a5*$^{fl/fl}$ Mice

Social interaction abnormalities have been suggested to arise from cortical excitation and inhibition imbalance (Yizhar et al., 2011), a correlation also observed in animals with abnormal regulation of translation (Gkogkas et al., 2013; Santini et al., 2013). We evaluated synaptic function in 21-day-old *Tie2*^{Cre};*Slc7a5*$^{fl/fl}$ mice using whole-cell recordings of pyramidal neurons in layer 2/3 of the somatosensory cortex. Examination of synaptic transmission revealed a slight increase in the amplitude of miniature excitatory postsynaptic currents (mEPSCs) and a marked reduction in the frequency of miniature inhibitory synaptic currents (mIPSCs) (Figured 4A and 4B), indicating a significant excitation and inhibition imbalance.

To determine whether the synaptic alterations in *Tie2*^{Cre};*Slc7a5*$^{fl/fl}$ mice are selective to the somatosensory cortex, we performed the same experiment in other brain regions. Given the locomotion abnormalities observed in *Tie2*^{Cre};*Slc7a5*$^{fl/fl}$ mice, we tested inputs received by the Purkinje cells. Similarly to the neocortex, *Tie2*^{Cre};*Slc7a5*$^{fl/fl}$ mouse cerebellar Purkinje cells display a significant reduction in mIPSC frequency (Figures S3C and S3D).

Changes in mIPSC frequency are generally due to differences in the number of functional synaptic sites and/or in the presynaptic release probability at existing sites (changes in the GABA vesicular pool or vesicular turnover rate). Therefore, we examined overall brain morphology (Figure S4A), cortical layering (Figure S4B), and inhibitory neuron distribution (Figure S4C) and found that for these parameters, somatosensory cortices of mutant animals were undistinguishable from the control. We further looked for differences in pre- and postsynaptic markers of inhibitory synapses. Importantly, we observed that the intensity of the vesicular GABA transporter (VGAT) staining, a marker for GABAergic presynaptic terminals, was lower in the somatosensory cortices of *Tie2*^{Cre};*Slc7a5*$^{fl/fl}$ mice (Figures 4C and S4D). However, the GABAergic postsynaptic marker neuroligin 2 (Varoqueaux et al., 2004) appeared qualitatively and quantitatively similar in the somatosensory cortex of the mutant and control mice (Figures 4D and S4E). The marked reduction of VGAT and normal neuroligin 2 protein levels in *Tie2*^{Cre};*Slc7a5*$^{fl/fl}$ mice were also confirmed by western blot analysis of cortical lysates (Figure 4E). To determine whether the reduction in VGAT staining intensity was due to a specific lessening of VGAT or a decline in the number of VGAT-containing vesicles, we analyzed inhibitory synapses by electron microscopy. In agreement with the electrophysiology results, we detected a significant reduction of vesicle number in symmetric synapses in the somatosensory cortices of *Tie2*^{Cre};*Slc7a5*$^{fl/fl}$ mice compared with control animals (Figure 4F).

Tie2^{Cre};*Slc7a5*$^{fl/fl}$ Mutant Mice Resemble *Bckdk* Knock Out Animals

The reduction in brain BCAA levels observed in *Tie2*^{Cre};*Slc7a5*$^{fl/fl}$ adult mice is comparable to what we measured in *Bckdk*$^{-/-}$ animals (Novarino et al., 2012). *Bckdk*$^{-/-}$ mice, in addition, display reduced-serum BCAA levels and a marked increase in brain

Figure 3. Neurobehavioral Abnormalities in the *Tie2*^{Cre};*Slc7a5*$^{fl/fl}$ Mice

(A–D) Decreased exploratory behavior and locomotion abnormalities in the *Tie2*^{Cre};*Slc7a5*$^{fl/fl}$ mice. (A) Open field test. Representative trajectories (left) and quantification of the total distance moved (middle) and the velocity (right) indicating that *Tie2*^{Cre};*Slc7a5*$^{fl/fl}$ mice are outperformed by controls; $^{**}p < 0.01$ (means ± SEM; n = 10 mice/genotype). (B) Comparison of the number of rearings pointing out deficiencies in the mutants; $^{**}p < 0.01$ (means ± SEM; n = 10 mice/genotype) (C) Walking beam performance on training days (day 1, day 2) and on the three trials of the test day (day 3), showing elevated latency to cross the beam in the mutants; $^{*}p < 0.05$, $^{**}p < 0.01$ (means ± SEM; n = 7 mice/genotype). (D) Representative images of control (left) and *Tie2*^{Cre};*Slc7a5*$^{fl/fl}$ strides (right) in the gait test. Forepaw (red) and hindpaw (blue).

(E) Altered gait of the *Tie2*^{Cre};*Slc7a5*$^{fl/fl}$ mice is evidenced by inter-genotype comparison of stride, sway, and stance length quantifications; $^{*}p < 0.05$, $^{**}p < 0.01$, $^{***}p < 0.001$ (means ± SEM; n = 7 mice/genotype).

(F) Three chamber social interaction test (left) and quantifications (right) of the number of contacts with the caged mouse (M) or with the caged object (O) revealing abnormal social interaction pattern in the mutant mice (mutants show no preference for the M over the O, as opposed to controls); $^{**}p < 0.01$; N.S., not significant (means ± SEM; n = 12 mice/genotype).

(G) Juvenile *Tie2*^{Cre};*Slc7a5*$^{fl/fl}$ mice display fewer reciprocal social interactions. *Slc7a5* mutant mice tend to stay farther apart from their cage mate (heatmap and bottom left graph) and exhibit fewer nose-to-nose contacts (bottom right graph). WT = *Slc7a5*$^{fl/+}$; KO = *Tie2*^{Cre};*Slc7a5*$^{fl/fl}$. $^{*}p < 0.05$ (means ± SEM; n = 8 mice/genotype).

(H) Isolation-induced USV at various postnatal days show that *Tie2*^{Cre};*Slc7a5*$^{fl/fl}$ mice emit an increased number of calls starting at P8. $^{*}p < 0.05$ (means ± SEM; n = 10 mice/genotype).

See also Figure S3.

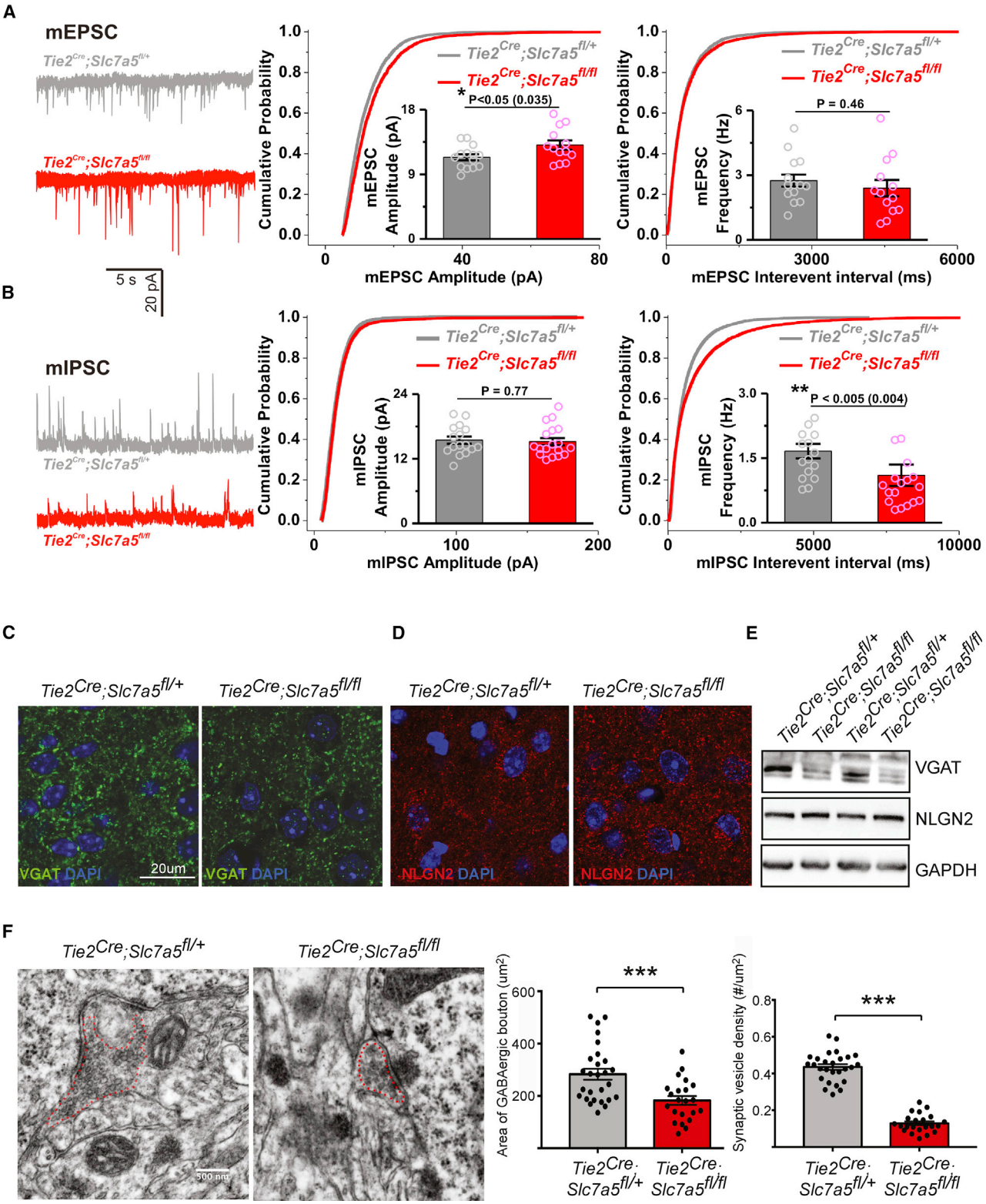

Figure 4. Excitation and Inhibition Imbalance in *Tie2*^{Cre};*Slc7a5*$^{fl/fl}$ Somatosensory Cortex

(A and B) Left: representative mEPSC (A) and mIPSC (B) recordings from *Tie2*^{Cre};*Slc7a5*$^{fl/+}$ and *Tie2*^{Cre};*Slc7a5*$^{fl/fl}$ somatosensory cortex (SCX) layers 2-3 pyramidal neurons; Right: cumulative probability distributions of peak amplitudes and inter-event intervals of mEPSC (A) and mIPSC (B) in the two genotypes.

(legend continued on next page)

levels of several other LNAAs (Novarino et al., 2012) but normal neurotransmitter concentrations (Figure S5G). Thus, it remained unclear whether neurological abnormalities in *BCKDK* mutant patients and mice are due to alterations in serum or brain BCAA. Alternatively, the pathological conditions observed in patients carrying mutations in *BCKDK* could be due to increased brain LNAA levels.

We compared *Bckdk*$^{-/-}$ and *Tie2*^{Cre};*Slc7a5*$^{fl/fl}$ mouse lines and observed a great phenotypic overlap. Similarly to *Tie2*^{Cre};*Slc7a5*$^{fl/fl}$ mice, *Bckdk* mutants show motor coordination abnormalities, autism-related behaviors, decreased mIPSC frequency (Figures S5A–S5F), and activation of the AAR pathway (Novarino et al., 2012) implying that *Bckdk*$^{-/-}$ and *Tie2*^{Cre};*Slc7a5*$^{fl/fl}$ mice share pathophysiological mechanisms.

SLC7A5 Mutations in Patients with ASD and Motor Delay

Given the essential role of *SLC7A5* in regulating brain BCAA homeostasis and the phenotypic overlap between *Bckdk* and *Slc7a5* mutant mice, we reasoned that mutations in *SLC7A5* could lead to ASD and motor abnormalities in humans. Thus, we collaboratively screened whole exome sequencing (WES) data from more than 2,000 families with documented parental consanguinity, presenting with children with various neurological diseases. We identified two independent families with multiple children affected by ASD, microcephaly, and motor problems all harboring homozygous missense mutations in the gene *SLC7A5*.

Family 1426 is a consanguineous family with two branches and five affected individuals (Figures 5A–5C). WES analysis of patients 1426-5 and 1426-19 (Figure 5A) identified a unique shared homozygous missense variant in the *SLC7A5* gene (Table S2). The homozygous mutation falls in a linkage pick with LOD score >4 (Figure S6A) and segregates with the disorder in the rest of the family (confirmed by Sanger sequencing). The A246V mutation changes a highly conserved alanine situated in a stretch of preserved amino acids predicted to be important for amino acid transport (Figures 6A and 6B). In an additional cohort of 1,000 neurodevelopmental disorder patients analyzed by WES, we identified Family 1465 including two patients with identical ASD, microcephaly, and motor delay (Figures 5A–5C) sharing a predicted deleterious homozygous mutation (Figure S6B) in *SLC7A5* leading to the change of the conserved proline in position 375 to a leucine (P375L) (Figure 6A). Both genetic variants were not present in more than 200 ethnically-matched, healthy control chromosomes, nor in our dataset of over 2,000 chromosomes or in publicly available databases (Table S2).

Functional Assessment of *SLC7A5* A246V and P375L Mutations

We mapped the two genetic variants onto a homology model of SLC7A5 (Geier et al., 2013). A246 is located in transmembrane helix 6 in close proximity to the extracellular side and to the channel (Figure 6B). Mutation of this residue to the larger valine is therefore likely to impact the transporter's structure by disrupting helix-helix packing and ligand transport. P375 is located in transmembrane helix 9 in close proximity to the cytoplasmic side (Figure 6B). Proline often plays a key role in introducing kinks in helices and allowing conformational changes important for transporter function. Thus, mutation of this residue to leucine is likely to disrupt the flexibility required for transport by SLC7A5.

To validate the functional impact of the A246V and P375L substitution, we performed transport assays. Therefore, the recombinant A246V and P375L mutant proteins were successfully expressed (Figure S7A), reconstituted in proteoliposomes (Figures 6C and 6D) and tested with a series of transport assays (Napolitano et al., 2015).

From transport time course analysis, it was evident that the mutant A246V was virtually inactive (Figure 6C). As predicted by the homology model (Figure 6B), the functional defect may be ascribed to a higher steric hindrance of the valine side chain with respect to that of alanine. To verify this hypothesis and that the functional change was specifically ascribed to the pathological variant, we analyzed an artificial mutant, A246G, (Figure S7A) in which the 246 side chain had been abolished. In contrast to the patient-specific A246V mutation, the A246G variant did not show any transport defect (Figures 6C and S7B). To exclude that the loss of activity observed in the A246V mutant could be due to reconstitution failing, we assessed the efficiency of protein reconstitution. We found no differences in the reconstitution of the A246V mutant compared to the WT protein (Figure S7A). Taken together, all the data confirmed that the substitution of A246V was functionally disruptive.

In contrast, the P375L mutant showed no significant variations in time-dependent activity and external K_M with respect to WT (Figures S7C and S7D). Owing to the location of P375 in an intracellular moiety of the protein (Figure 6B), we determined also the internal K_M for this mutant (~25 mM; 27 ± 9.9) (Figure S7E). Interestingly, the K_M value was approximately five times that of the WT (~5 mM; 5.2 ± 2.3), suggesting that some variations in the substrate binding/translocation pathway may occur upon mutation. We further performed efflux experiments for evaluating possible differences in the antiport reaction catalyzed by

Insets: quantifications of mean amplitudes and mean frequencies of the corresponding currents with significant differences in mutants versus controls. D = 0.093, $p < 10^{-11}$ (mEPSC amplitudes) and D = 0.099, $p < 10^{-15}$ (mIPSC interevent intervals); (means ± SEM, $n_{cells}/n_{animals}$/genotype: 14/7/*Tie2*^{Cre};*Slc7a5*$^{fl/+}$ and 13/5/*Tie2*^{Cre};*Slc7a5*$^{fl/fl}$ (mEPSC); 16/7/*Tie2*^{Cre};*Slc7a5*$^{fl/+}$ and 18/5/*Tie2*^{Cre};*Slc7a5*$^{fl/fl}$ (mIPSC).

(C) Representative confocal images of VGAT-positive synaptic puncta (green) in control (left) and *Tie2*^{Cre};*Slc7a5*$^{fl/fl}$ (right) cortical sections displaying decreased staining intensity in the mutants. Nuclei were stained with DAPI (blue).

(D) Confocal imaging of cortical sections labeled for neuroligin 2 (NLGN2, red) of control (left) and *Tie2*^{Cre};*Slc7a5*$^{fl/fl}$ (right) animals revealing no difference between genotypes. Nuclei were stained with DAPI (blue). Scale bar as in (C).

(E) Western blot analysis from cortical lysates indicating decreased VGAT (top) and similar NLGN2 protein levels (middle) in *Tie2*^{Cre};*Slc7a5*$^{fl/fl}$ mice compared with controls. GAPDH (bottom) was used as internal control.

(F) Electron microscopy imaging of the SCX layers 2-3 showing that *Tie2*^{Cre};*Slc7a5*$^{fl/fl}$ mice have a decreased area of GABAergic boutons and decreased density of vesicles per bouton. Typical micrograph images (left), summary graphs of presynaptic area (middle), and vesicle density (right); ***$p < 0.001$ (means ± SEM; $n_{synapses}$/genotype: 27/control and 22/mutant).

See also Figures S4 and S5.

A

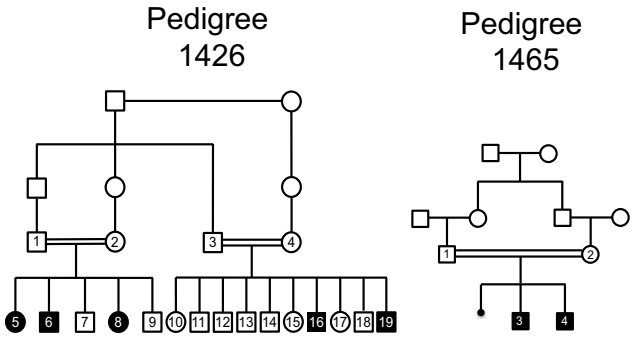

B

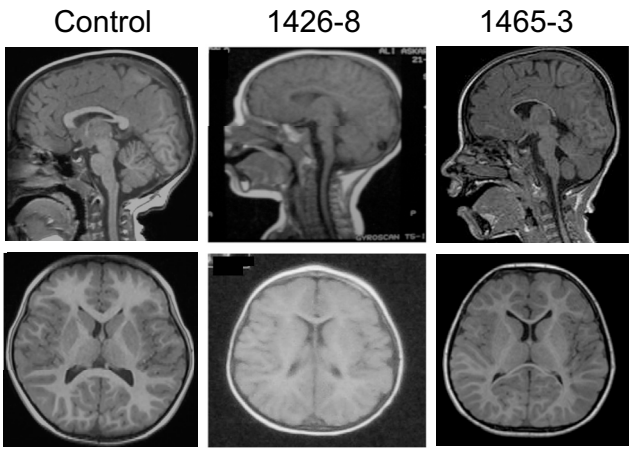

C

Patient	1426-5	1426-6	1426-8	1426-19	1465-3	1465-4
Gender	F	M	F	M	M	M
Origin	Libya	Libya	Libya	Libya	Turkish	Turkish
Age at diagnosis	N/A	N/A	5 months	N/A	2 weeks	5-6 months
HC at birth (SD)	N/A	-2/-3	N/A	N/A	- 3	- 3
HC at latest examination (SD)	-5	-2,3	-5,5	-5	N/A	N/A
Developmental milestones						
Gross motor (normal/delayed/absent)	Delayed	Delayed	Delayed	Delayed	Delayed	Delayed
Fine motor (normal/delayed/absent)	Delayed	Delayed	Delayed	Delayed	Delayed	Delayed
Language (normal/delayed/absent)	Delayed	Delayed	Delayed	Delayed	Absent	Absent
Social (normal/delayed/absent)	Delayed	Delayed	Delayed	Delayed	Delayed	Delayed
Seizure						
Type	-	-	-	N/A	GTC	GTC
Onset	-	-	-	N/A	1year	6 months
Autism associated disorder						
Impaired social interactions	+	+	+	N/A	+	+
Impaired eye-to-eye gaze, facial expression	+	+	+	N/A	+	+
Impaired ability to form peer relationships	+	+	+	N/A	+	+
Lack of spontaneous play	+	+	+	N/A	+	+
Restrictive behavior, interests and activities	+	+	+	N/A	+	+
Stereotyped, repetitive behavior	-	-	-	N/A	+	+
Inflexible adherence to routines or rituals	+	+	+	N/A	+	+
Additional CNS investigations						
MRI	N/A	Cortical atrophy	Normal	N/A	Thin CC	Thin CC

Figure 5. Mutations in the Human *SLC7A5* Lead to ASD and Motor Deficits

(A) *SLC7A5* mutations identified in families 1426 and 1465 in individuals with ASD, motor deficits, and microcephaly. Pedigrees 1426 and 1465 display first-cousin consanguinity, five, and two affected patients (solid symbols), respectively and unaffected members (open symbols).

(B) MRI from one patient for each family showing microcephaly and thin corpus callosum but normal axial T1 sequence of the brain. Control child brain MRIs were obtained from unrelated individuals.

(C) Clinical presentation of patients from family 1426 and 1465. HC, head circumference; SD, standard deviation; GTC, generalized tonic clonic; N/A not available; CC, corpus callosum.

See also Table S2.

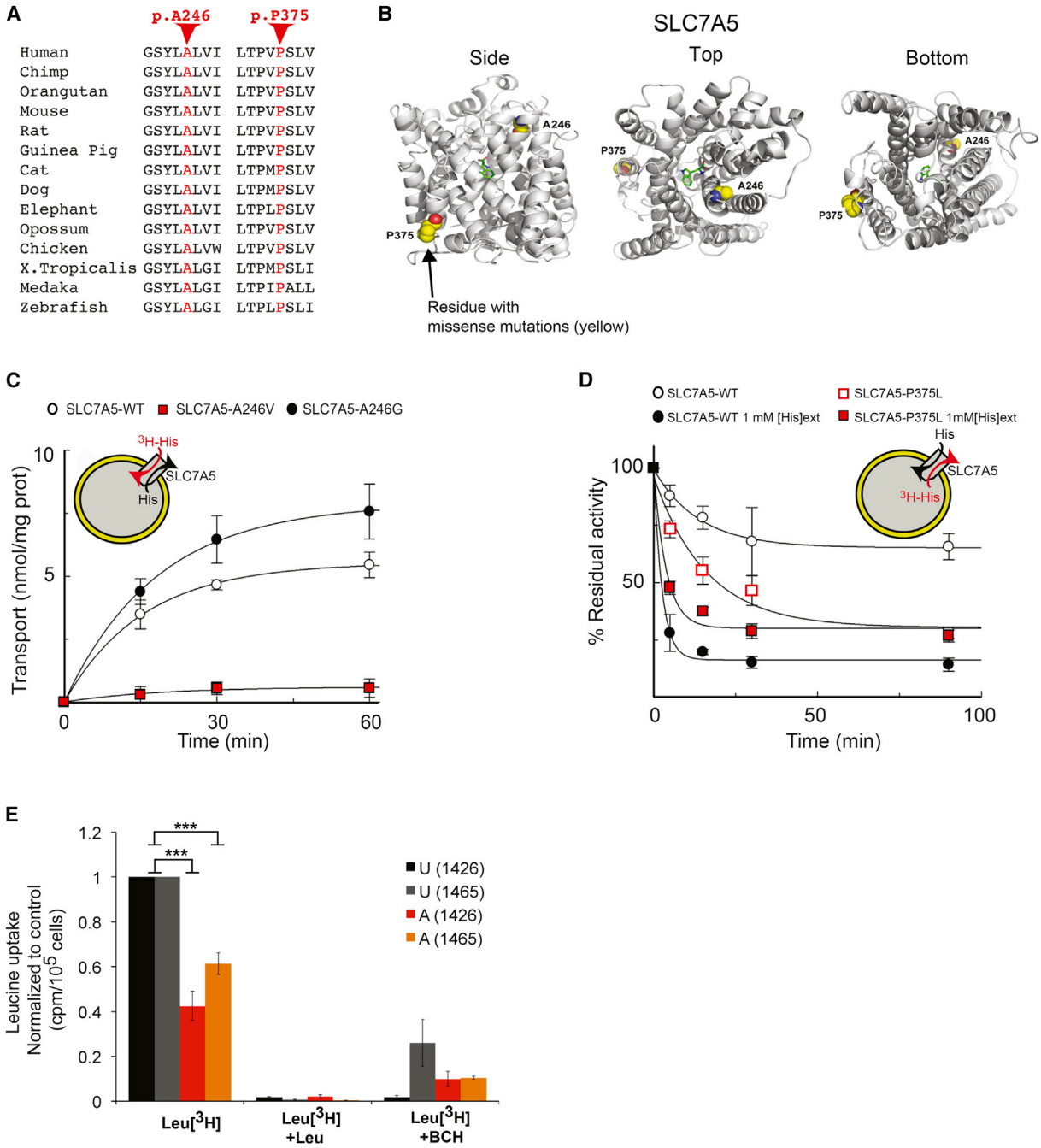

Figure 6. A246V and P375L Mutations Compromise SLC7A5 Function

(A) Conservation of the SLC7A5 A246 and P375 in several species.

(B) Side, top, and bottom views of the predicted structure of SLC7A5 in complex with tryptophan showing SLC7A5 backbone atoms (gray ribbon), atoms of the residues constituting the missense mutations (yellow spheres) and the ligand tryptophan (green sticks), oxygen atoms (red), and nitrogen atoms (blue).

(C) SLC7A5 wild-type, A246V, and A246G mutants overexpressed and purified by fast protein liquid chromatography were reconstituted in proteoliposomes. Transport is followed as uptake (red arrow) of external [^{3}H]His in exchange with internal His. Transport was started by adding external 5 μM [^{3}H]His at time zero to proteoliposomes containing 10 mM His reconstituted with SLC7A5-WT (○), SLC7A5-A246V (solid red square) or SLC7A5-A246G (●) and stopped at the indicated times (means ± SD; n = 5 experiments).

(D) Time-dependence of [^{3}H]His efflux from proteoliposomes reconstituted with SLC7A5-WT or SLC7A5-P375L was measured. Proteoliposomes reconstituted with SLC7A5-WT (○, ●) or SLC7A5-P375L (open red square, closed red square), containing 2 mM His were radioactivity-preloaded. Efflux was measured in absence (○, open red square; uniport) or presence of external 1 mM His (●, solid red square; antiport). Percentage of His efflux was calculated with respect to time 0 (means ± SD; n = 4 experiments).

(legend continued on next page)

SLC7A5. The measurements were performed using intraliposomal histidine concentration (2 mM), to create conditions similar to the intracellular environment. Surprisingly, the mutant P375L was mostly uncoupled. Indeed, while WT showed a very slow efflux in absence of external substrate, according to its antiport mode, the mutant unidirectional efflux was much faster with a nearly complete proteoliposome emptying (Figure 6D). The anomaly observed in the P375L mutant indicates that, in vivo, loss of intracellular SLC7A5 substrate(s) impairs the driving force for taking up SLC7A5 substrates.

To further validate the functional impact of SLC7A5 mutation in the patient-specific genetic background, we obtained human dermal fibroblasts from two affected and a few unaffected members of Family 1426 and Family 1465 and performed [^{3}H]-leucine uptake assay (Sinclair et al., 2013). SLC7A5 transcript is expressed in human dermal fibroblasts and its level is not affected by the missense mutations (Figure S7F). Cells carrying the homozygous A246V or P375L variant, however, show a significant reduction in [^{3}H]-leucine uptake when compared with control cells (Figure 6E). Thus, the substitution of the SLC7A5 alanine 246 into a valine, or of the proline 375 into a leucine, is sufficient to significantly reduce the SLC7A5-mediated BCAA uptake.

BCAA Intracerebroventricular Injections Rescue Neurological Abnormalities in Adult *Slc7a5* Mutant Mice

The identification of ASD patients carrying mutations in the *SLC7A5* gene prompted the question whether this condition is potentially treatable. Therefore, we injected leucine and isoleucine stereotaxically into the brain of adult *Tie2*^{Cre}*;Slc7a5*$^{fl/fl}$ mice for 3 weeks (Figure 7A). Injected mice were then tested for some of the behavioral phenotypes described in Figure 3 and brain amino acid levels. Notably, after 3 weeks of i.c.v. leucine and isoleucine delivery (Figure 7A), their brain level was normalized (Figure 7B; Table S3), and the mutant mice showed a significant improvement in neurobehavioral abnormalities. Specifically, we observed a decreased number of *Tie2*^{Cre}*;Slc7a5*$^{fl/fl}$ mice showing the clasping (50% of injected versus 89% of non-injected mutant mice) and the kyphosis phenotype (25% of injected versus 44% of non-injected mutant mice). Most importantly, we could not detect any difference between treated *Tie2*^{Cre}*;Slc7a5*$^{fl/fl}$ and wild-type mice in the open field test neither in velocity and distance moved nor in the number of rearings (Figure 7C). The gait of the injected *Tie2*^{Cre}*;Slc7a5*$^{fl/fl}$ mice was improved with a complete normalization of the sway length (Figure 7D). Importantly, wild-type animals injected with the leucine/isoleucine mixture were indistinguishable from the non-injected animals of the corresponding genotype (Figures 7C and 7D), indicating that leucine and isoleucine specifically improve behavior of *Slc7a5* mutants. Worth mentioning is the fact that the rescue of the social and vocalization abnormalities could not be tested given technical issues presented by the presence of the implanted pump and the size of the animals (see the STAR Methods).

Although further tests are required to determine the extent and efficacy of the treatment, our data suggest that certain neurobehavioral abnormalities observed in *Slc7a5* mutants can be rescued by i.c.v. administration of leucine and isoleucine in adulthood. Even if we cannot entirely disregard a role of the increased level of other amino acids, these results support the idea that the reduction in brain leucine and isoleucine levels is the determinant factor in the appearance of the neurological phenotypes observed in humans and mice lacking *SLC7A5* expression.

DISCUSSION

Although SLC7A5 has been described as a BBB amino acid transporter, studies accurately verifying its expression or examining its function at the BBB are completely missing in the literature. Moreover, transport studies were performed using only in vitro systems thus lacking the expression of other carriers with possibly overlapping substrates and its physiological importance remained almost completely undetermined.

Our study shows that *SLC7A5* loss of function leads to ASD and motor dysfunctions in humans and mice. This fits with our previous work in which we have shown that mutations implicated in abnormal BCAA catabolism lead to ASD and fine motor coordination problems (Novarino et al., 2012). Along the same line, an increase in the brain levels of these same amino acids leads to the maple syrup urine disorder, characterized by cognitive dysfunctions, seizures, and hypotonia (Menkes et al., 1954; Zinnanti et al., 2009). Although we acknowledge that ASD due to *SLC7A5* mutations may be an extremely rare condition, the present study indicates that fine-tuning of brain BCAA and LNAA concentrations is key for normal brain function, and mutations affecting genes contributing to BCAA homeostasis and the downstream signaling cascade may underlie a larger subgroup of ASD. In addition, this work has several important pathophysiological implications.

We show that *Slc7a5* expression at the BBB is particularly important to set a correct brain BCAA concentration. In fact, a lack of *Slc7a5* expression at the BBB leads to a significant reduction in brain BCAA levels, particularly leucine and isoleucine. Surprisingly, we did not detect significant reductions in the brain levels of the other LNAAs, which in the mutant mice are rather slightly increased, indicating that additional carriers are involved in their transport. Among the most altered amino acids, beside leucine and isoleucine, we detected histidine, suggesting that this amino acid may have a special role in the function of the transporter. Noteworthy, the normal brain histamine levels (Figure S2C), as well as the RNA-seq data obtained from mutant mice, exclude an alteration of histaminergic transmission. Moreover, abnormally high serum and cerebrospinal fluid histidine levels have been reported in healthy individuals implying that increased histidine concentration is non-pathological (Lam et al., 1996).

Furthermore, we show that deletion of *Slc7a5* from the BBB leads to activation of the AAR pathway and reduced

(E) Radio-labeled leucine ([^{3}H]Leu) transport analysis in human fibroblasts from affected (A) and unaffected (U) members of families 1426 and 1465 illustrating a significant reduction in leucine uptake by the cells of affected patients. Specificity of leucine uptake was assessed by competition with 10 mM cold leucine (Leu) or 10 mM 2 BCH; ***$p < 0.001$ (means ± SEM; $N \geq 3$ experiments performed with fibroblasts from two patients and one healthy control/family).
See also Figure S7.

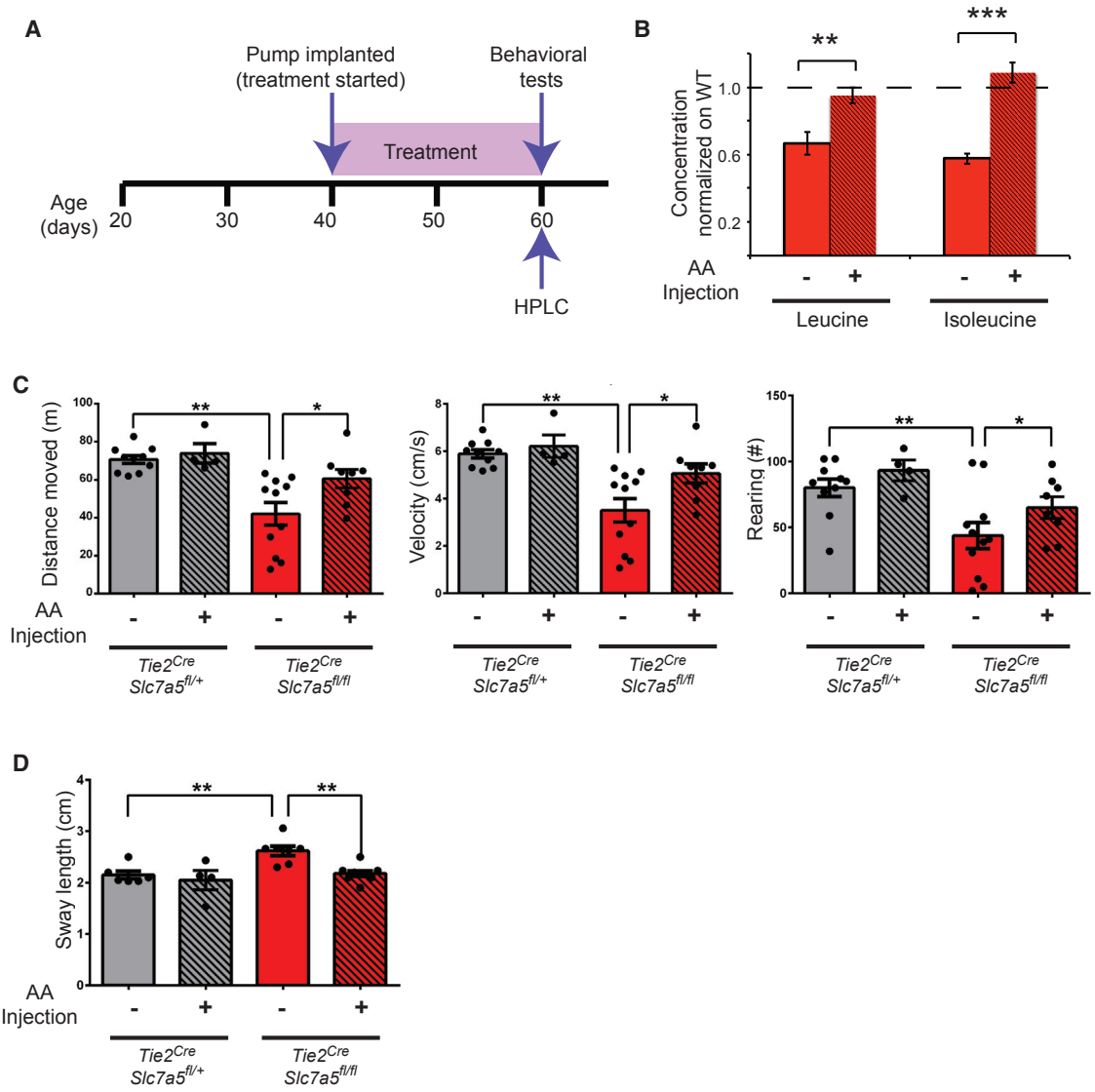

Figure 7. Normalization of *Tie2*^{Cre};*Slc7a5*$^{fl/fl}$ Mouse Behavior after Leucine and Isoleucine i.c.v. Administration

(A) Timeline of treatment and HPLC and behavioral tests.

(B) Brain levels of leucine (left) and isoleucine (right) in age-matched animals receiving (+) or not receiving (−) the i.c.v. treatment. Amino acid levels were normalized to protein concentration and to wild-type levels. **p < 0.01, ***p < 0.001 (means ± SEM; n = 8 mice/genotype).

(C) Quantification of the total distance moved (left), velocity (middle), and number of rearings (right) in the open field revealing similar behavior in treated (+) *Tie2*^{Cre};*Slc7a5*$^{fl/fl}$ mice and non-treated (−) or treated (+) controls (*Tie2*^{Cre};*Slc7a5*$^{fl/+}$) but significant differences with non-treated (−) *Tie2*^{Cre};*Slc7a5*$^{fl/fl}$ mice. *p < 0.05, **p < 0.01 (means ± SEM; n = 10 (−) control, n = 4 (+) control, n = 11 (−) mutant, and n = 8 (+) mutant).

(D) Similar sway length in treated (+) mutant mice and non-treated (−) or treated (+) control (*Tie2*^{Cre};*Slc7a5*$^{fl/+}$) animals but significant difference with non-treated (−) *Tie2*^{Cre};*Slc7a5*$^{fl/fl}$ mice. **p < 0.01 (means ± SEM; n = 10 (−) control, n = 4 (+) control, n = 11 (−) mutant, and n = 8 (+) mutant).

See also Table S3.

cap-dependent translation. How exactly abnormal regulation of translation leads to the observed phenotypes in *SLC7A5* mutant humans and mice remains to be investigated. However, we observed that inhibitory neurons may be more sensitive to altered amino acid levels as Atf5, a key molecule in the AAR pathway, has been reported to be preferentially expressed in GABA-synthetizing neurons (Zeisel et al., 2015). Accordingly, we found that deletion of *Slc7a5* from the BBB is sufficient to reduce cortical inhibitory activity, resulting in cortical excitation and inhibition imbalance and probably causing the observed neurological complications. Similarly, most of the functionally characterized ASD-mutations lead to an imbalance in the excitation/inhibition ratio. Thus, drugs acting on GABA transmission are considered an opportunity for the treatment of ASD and epilepsy (Braat and Kooy, 2015). It is therefore tempting to reason that identifying the rules by which simple molecule such as the BCAAs may regulate GABAergic transmission might have a crucial impact on the development of novel therapeutic strategies for ASD.

Notably, besides representing a new subgroup of ASD, BCAA-related ASD may also represent a group of treatable conditions. Indeed, BCAA dietary administration in *BCKDK* null mice and humans (Novarino et al., 2012), as well as leucine and isoleucine i.c.v. injection in adult *Tie2*^{Cre};*Slc7a5*$^{fl/fl}$ mice lead to a significant improvement of the neurobehavioral abnormalities.

STAR★METHODS

Detailed methods are provided in the online version of this paper and include the following:

- KEY RESOURCES TABLE
- CONTACT FOR REAGENT AND RESOURCE SHARING
- EXPERIMENTAL MODEL AND SUBJECT DETAILS
  - Mice
  - Human Subjects and Sample Collection
  - Cell Lines
  - Protein Model
- METHOD DETAILS
  - Amino Acid Analysis
  - RNA-Sequencing
  - Western Blot
  - Polysome Profiling
  - Immunohistochemistry
  - Nissl Staining
  - Electrophysiology
  - Electron Microscopy
  - Behavioral Studies
  - Intracerebroventricular Dye Injection
  - Serial Surgical Implantation of Cannula and Osmotic Pumps
  - Whole Exome Sequencing, Homozygosity Profile, and Variant Prioritization
  - Sanger Sequencing
  - Leucine Uptake Assay
  - Cloning, Mutagenesis, and Expression of the Human SLC7A5 Wild-Type and Mutants
  - Purification of Human SLC7A5 Wild-Type and Mutants
  - Reconstitution of Human SLC7A5 Wild-Type and Mutants in Proteoliposomes
  - Transport Measurements
  - Ultracentrifugation of Proteoliposomes
- QUANTIFICATION AND STATISTICAL ANALYSIS
  - Amino Acid Data
  - RNA-Sequencing
  - Protein Data
  - Neuronal Data
  - Electron Microscopy
  - Behavior
  - Transport Measurement Data
- DATA AND SOFTWARE AVAILABILITY
  - Data Resources
- ADDITIONAL RESOURCES

SUPPLEMENTAL INFORMATION

Supplemental Information includes seven figures and five tables and can be found with this article online at http://dx.doi.org/10.1016/j.cell.2016.11.013.

AUTHOR CONTRIBUTIONS

D.C.T., E.D., C.P.D., M. Tesulov, E.M., A.J., and G.N. performed experiments. G.N. conceived and supervised the study. M.K., F.M.S., K.B., M. Topcu, S.E., T.B.-O., A.O.C., M.G., and J.G.G. recruited and characterized patients. A.O.C. and G.N. performed and analyzed WES. D.C.T., P.C.J., and K.D., performed polysome experiments. M.S., M.G., and C.I., performed protoliposome experiments. A.S. performed in silico analysis. R.O. and Y.K., generated and tested LAT1 antibody. G.N. wrote the paper together with D.C.T, E.D., and C.P.D. All authors read and approved the final version of the manuscript.

ACKNOWLEDGMENTS

We thank A.C. Manzano, Mike Liu, and F. Marr for technical assistance, and R. Shigemoto and the IST Austria Electron Microscopy (EM) Facility for assistance. We acknowledge support from CIDR for genome-wide SNP analysis (X01HG008823) and Broad Institute Center for Mendelian Disorders (UM1HG008900 to D. MacArthur), the Yale Center for Mendelian Disorders (U54HG006504 to M.G.), the Gregory M. Kiez and Mehmet Kutman Foundation (M.G.), Italian Ministry of Instruction University and Research (PON01_00937 to C.I.), and NIH (R01-GM108911 to A.S.). This work was supported by NICHD (P01HD070494) and SFARI (grant 275275) to J.G.G., and FWF (SFB35_3523) to G.N.

Received: September 8, 2016
Revised: October 18, 2016
Accepted: November 3, 2016
Published: December 1, 2016

REFERENCES

Angelastro, J.M., Ignatova, T.N., Kukekov, V.G., Steindler, D.A., Stengren, G.B., Mendelsohn, C., and Greene, L.A. (2003). Regulated expression of ATF5 is required for the progression of neural progenitor cells to neurons. J. Neurosci. *23*, 4590–4600.

Bailey, A., Le Couteur, A., Gottesman, I., Bolton, P., Simonoff, E., Yuzda, E., and Rutter, M. (1995). Autism as a strongly genetic disorder: evidence from a British twin study. Psychol. Med. *25*, 63–77.

Banko, J.L., and Klann, E. (2008). Cap-dependent translation initiation and memory. Prog. Brain Res. *169*, 59–80.

Braat, S., and Kooy, R.F. (2015). The GABAA receptor as a therapeutic target for neurodevelopmental disorders. Neuron *86*, 1119–1130.

Braun, L.D., Cornford, E.M., and Oldendorf, W.H. (1980). Newborn rabbit blood-brain barrier is selectively permeable and differs substantially from the adult. J. Neurochem. *34*, 147–152.

Carter, R.J., Morton, J., and Dunnett, S.B. (2001). Motor coordination and balance in rodents. Curr. Prot. Neurosci. *Chapter 8*, Unit 8.12.

Chen, A., Muzzio, I.A., Malleret, G., Bartsch, D., Verbitsky, M., Pavlidis, P., Yonan, A.L., Vronskaya, S., Grody, M.B., Cepeda, I., et al. (2003). Inducible enhancement of memory storage and synaptic plasticity in transgenic mice expressing an inhibitor of ATF4 (CREB-2) and C/EBP proteins. Neuron *39*, 655–669.

Depristo, M.A., Banks, E., Poplin, R., Garimella, K.V., Maguire, J.R., Hartl, C., Philippakis, A.A., del Angel, G., Rivas, M.A., Hanna, M., et al. (2011). A framework for variation discovery and genotyping using next-generation DNA sequencing data. Nat Genet. *43*, 491–598.

De Rubeis, S., He, X., Goldberg, A.P., Poultney, C.S., Samocha, K., Cicek, A.E., Kou, Y., Liu, L., Fromer, M., Walker, S., et al.; DDD Study; Homozygosity Mapping Collaborative for Autism; UK10K Consortium (2014). Synaptic, transcriptional and chromatin genes disrupted in autism. Nature *515*, 209–215.

Deacon, R.M. (2006). Digging and marble burying in mice: simple methods for in vivo identification of biological impacts. Nat. Protoc. *1*, 122–124.

del Amo, E.M., Urtti, A., and Yliperttula, M. (2008). Pharmacokinetic role of L-type amino acid transporters LAT1 and LAT2. Eur. J. Pharm. Sci. *35*, 161–174.

DeLano, W.L. (2002). Unraveling hot spots in binding interfaces: progress and challenges. Curr. Opin. Struct. Biol. *12*, 14–20.

DeVos, S.L., and Miller, T.M. (2013). Direct intraventricular delivery of drugs to the rodent central nervous system. J. Vis. Exp. *75*, e50326.

Dobin, A., Davis, C.A., Schlesinger, F., Drenkow, J., Zaleski, C., Jha, S., Batut, P., Chaisson, M., and Gingeras, T.R. (2013). STAR: ultrafast universal RNA-seq aligner. Bioinformatics *29*, 15–21.

Falcon, S., and Gentleman, R. (2007). Using GOstats to test gene lists for GO term association. Bioinformatics *23*, 257–258.

Folstein, S., and Rutter, M. (1977). Genetic influences and infantile autism. Nature *265*, 726–728.

Fotiadis, D., Kanai, Y., and Palacín, M. (2013). The SLC3 and SLC7 families of amino acid transporters. Mol. Aspects Med. *34*, 139–158.

Galluccio, M., Amelio, L., Scalise, M., Pochini, L., Boles, E., and Indiveri, C. (2012). Over-expression in E. coli and purification of the human OCTN2 transport protein. Mol. Biotechnol. *50*, 1–7.

Galluccio, M., Pingitore, P., Scalise, M., and Indiveri, C. (2013). Cloning, large scale over-expression in E. coli and purification of the components of the human LAT 1 (SLC7A5) amino acid transporter. Protein J. *32*, 442–448.

Galluccio, M., Pochini, L., Peta, V., Ianni, M., Scalise, M., and Indiveri, C. (2015). Functional and molecular effects of mercury compounds on the human OCTN1 cation transporter: C50 and C136 are the targets for potent inhibition. Toxicol. Sci. *144*, 105–113.

Gao, X., Zhou, L., Jiao, X., Lu, F., Yan, C., Zeng, X., Wang, J., and Shi, Y. (2010). Mechanism of substrate recognition and transport by an amino acid antiporter. Nature *463*, 828–832.

Geier, E.G., Schlessinger, A., Fan, H., Gable, J.E., Irwin, J.J., Sali, A., and Giacomini, K.M. (2013). Structure-based ligand discovery for the large-neutral amino acid transporter 1, LAT-1. Proc. Natl. Acad. Sci. USA *110*, 5480–5485.

Gkogkas, C.G., Khoutorsky, A., Ran, I., Rampakakis, E., Nevarko, T., Weatherill, D.B., Vasuta, C., Yee, S., Truitt, M., Dallaire, P., et al. (2013). Autism-related deficits via dysregulated eIF4E-dependent translational control. Nature *493*, 371–377.

Gnirke, A., Melnikov, A., Maguire, J., Rogov, P., LeProust, E.M., Brockman, W., Fennell, T., Giannoukos, G., Fisher, S., Russ, C., et al. (2009). Solution hybrid selection with ultra-long oligonucleotides for massively parallel targeted sequencing. Nat. Biotechnol. *27*, 182–189.

Green, T.A., Alibhai, I.N., Unterberg, S., Neve, R.L., Ghose, S., Tamminga, C.A., and Nestler, E.J. (2008). Induction of activating transcription factors (ATFs) ATF2, ATF3, and ATF4 in the nucleus accumbens and their regulation of emotional behavior. J. Neurosci. *28*, 2025–2032.

Guyenet, S.J., Furrer, S.A., Damian, V.M., Baughan, T.D., La Spada, A.R., and Garden, G.A. (2010). A simple composite phenotype scoring system for evaluating mouse models of cerebellar ataxia. J. Vis. Exp. *39*, 1787.

Kilberg, M.S., Shan, J., and Su, N. (2009). ATF4-dependent transcription mediates signaling of amino acid limitation. Trends Endocrinol. Metab. *20*, 436–443.

Kisanuki, Y.Y., Hammer, R.E., Miyazaki, J., Williams, S.C., Richardson, J.A., and Yanagisawa, M. (2001). Tie2-Cre transgenic mice: a new model for endothelial cell-lineage analysis in vivo. Dev. Biol. *230*, 230–242.

Lam, W.K., Cleary, M.A., Wraith, J.E., and Walter, J.H. (1996). Histidinaemia: a benign metabolic disorder. Arch. Dis. Child. *74*, 343–346.

Lefauconnier, J.M., and Trouvé, R. (1983). Developmental changes in the pattern of amino acid transport at the blood-brain barrier in rats. Brain Res. *282*, 175–182.

Love, M.I., Huber, W., and Anders, S. (2014). Moderated estimation of fold change and dispersion for RNA-seq data with DESeq2. Genome Biol. *15*, 550.

Mastroberardino, L., Spindler, B., Pfeiffer, R., Skelly, P.J., Loffing, J., Shoemaker, C.B., and Verrey, F. (1998). Amino-acid transport by heterodimers of 4F2hc/CD98 and members of a permease family. Nature *395*, 288–291.

Matsuo, H., Tsukada, S., Nakata, T., Chairoungdua, A., Kim, D.K., Cha, S.H., Inatomi, J., Yorifuji, H., Fukuda, J., Endou, H., and Kanai, Y. (2000). Expression of a system L neutral amino acid transporter at the blood-brain barrier. Neuroreport *11*, 3507–3511.

Menkes, J.H., Hurst, P.L., and Craig, J.M. (1954). A new syndrome: progressive familial infantile cerebral dysfunction associated with an unusual urinary substance. Pediatrics *14*, 462–467.

Moy, S.S., Nadler, J.J., Young, N.B., Perez, A., Holloway, L.P., Barbaro, R.P., Barbaro, J.R., Wilson, L.M., Threadgill, D.W., Lauder, J.M., et al. (2007). Mouse behavioral tasks relevant to autism: phenotypes of 10 inbred strains. Behav. Brain Res. *176*, 4–20.

Napolitano, L., Scalise, M., Galluccio, M., Pochini, L., Albanese, L.M., and Indiveri, C. (2015). LAT1 is the transport competent unit of the LAT1/CD98 heterodimeric amino acid transporter. Int. J. Biochem. Cell Biol. *67*, 25–33.

Novarino, G., El-Fishawy, P., Kayserili, H., Meguid, N.A., Scott, E.M., Schroth, J., Silhavy, J.L., Kara, M., Khalil, R.O., Ben-Omran, T., et al. (2012). Mutations in BCKD-kinase lead to a potentially treatable form of autism with epilepsy. Science *338*, 394–397.

Romano, E., Michetti, C., Caruso, A., Laviola, G., and Scattoni, M.L. (2013). Characterization of neonatal vocal and motor repertoire of reelin mutant mice. PLoS ONE *8*, e64407.

Saier, M.H., Jr., Yen, M.R., Noto, K., Tamang, D.G., and Elkan, C. (2009). The Transporter Classification Database: recent advances. Nucleic Acids Res. *37*, D274–D278.

Santini, E., Huynh, T.N., MacAskill, A.F., Carter, A.G., Pierre, P., Ruggero, D., Kaphzan, H., and Klann, E. (2013). Exaggerated translation causes synaptic and behavioural aberrations associated with autism. Nature *493*, 411–415.

Scalise, M., Pochini, L., Panni, S., Pingitore, P., Hedfalk, K., and Indiveri, C. (2014). Transport mechanism and regulatory properties of the human amino acid transporter ASCT2 (SLC1A5). Amino Acids *46*, 2463–2475.

Scattoni, M.L., Crawley, J., and Ricceri, L. (2009). Ultrasonic vocalizations: a tool for behavioural phenotyping of mouse models of neurodevelopmental disorders. Neurosci. Biobehav. Rev. *33*, 508–515.

Seelow, D., Schuelke, M., Hildebrandt, F., and Nurnberg, P. (2009). HomozygosityMapper- an interactive approach to homozygosity mapping. Nucleic Acids Res. *37*, W593–W599.

Silverman, J.L., Turner, S.M., Barkan, C.L., Tolu, S.S., Saxena, R., Hung, A.Y., Sheng, M., and Crawley, J.N. (2011). Sociability and motor functions in Shank1 mutant mice. Brain Res. *1380*, 120–137.

Sinclair, L.V., Rolf, J., Emslie, E., Shi, Y.B., Taylor, P.M., and Cantrell, D.A. (2013). Control of amino-acid transport by antigen receptors coordinates the metabolic reprogramming essential for T cell differentiation. Nat. Immunol. *14*, 500–508.

Trinh, M.A., Kaphzan, H., Wek, R.C., Pierre, P., Cavener, D.R., and Klann, E. (2012). Brain-specific disruption of the eIF2α kinase PERK decreases ATF4 expression and impairs behavioral flexibility. Cell Rep. *1*, 676–688.

Varoqueaux, F., Jamain, S., and Brose, N. (2004). Neuroligin 2 is exclusively localized to inhibitory synapses. Eur. J. Cell Biol. *83*, 449–456.

Verrey, F. (2003). System L: heteromeric exchangers of large, neutral amino acids involved in directional transport. Pflugers Arch. *445*, 529–533.

Wang, Q., Bailey, C.G., Ng, C., Tiffen, J., Thoeng, A., Minhas, V., Lehman, M.L., Hendy, S.C., Buchanan, G., Nelson, C.C., et al. (2011). Androgen receptor and nutrient signaling pathways to coordinate the demand for increased amino acid transport during prostate cancer progression. Cancer Res. *71*, 7526–7536.

Watson, R.E., Desesso, J.M., Hurtt, M.E., and Cappon, G.D. (2006). Postnatal growth and morphological development of the brain: a species comparison. Birth Defects Res. B Dev. Reprod. Toxicol. *77*, 471–484.

Wolfson, R.L., Chantranupong, L., Saxton, R.A., Shen, K., Scaria, S.M., Cantor, J.R., and Sabatini, D.M. (2016). Sestrin2 is a leucine sensor for the mTORC1 pathway. Science *351*, 43–48.

Yizhar, O., Fenno, L.E., Prigge, M., Schneider, F., Davidson, T.J., O'Shea, D.J., Sohal, V.S., Goshen, I., Finkelstein, J., Paz, J.T., et al. (2011). Neocortical excitation/inhibition balance in information processing and social dysfunction. Nature *477*, 171–178.

Zeisel, A., Muñoz-Manchado, A.B., Codeluppi, S., Lönnerberg, P., La Manno, G., Juréus, A., Marques, S., Munguba, H., He, L., Betsholtz, C., et al. (2015). Brain structure. Cell types in the mouse cortex and hippocampus revealed by single-cell RNA-seq. Science *347*, 1138–1142.

Zinnanti, W.J., Lazovic, J., Griffin, K., Skvorak, K.J., Paul, H.S., Homanics, G.E., Bewley, M.C., Cheng, K.C., Lanoue, K.F., and Flanagan, J.M. (2009). Dual mechanism of brain injury and novel treatment strategy in maple syrup urine disease. Brain *132*, 903–918.

STAR★METHODS

KEY RESOURCES TABLE

REAGENT or RESOURCE	SOURCE	IDENTIFIER
Antibodies		
Rabbit monoclonal anti-4E-BP1	Cell Signaling Technology	Cat#9644S; RRID: AB_10691384
Rabbit monoclonal anti-Phospho-4E-BP1	Cell Signaling Technology	Cat#2855S; RRID: AB_560835
Rabbit monoclonal anti-eIF4E	Cell Signaling Technology	Cat#2067S; RRID: AB_2097675
Rabbit polyclonal anti-Phospho-eIF4E	Cell Signaling Technology	Cat#9741S; RRID: AB_331677
Rabbit polyclonal anti-eIF2 alpha	Cell Signaling Technology	Cat#9722S; RRID: AB_2230924
Rabbit monoclonal anti-Phospho-eIF2 alpha	Cell Signaling Technology	Cat#3398S; RRID: AB_2096481
Rabbit monoclonal anti-S6K	Cell Signaling Technology	Cat#2708S; RRID: AB_390722
Rabbit monoclonal anti-Phospho-S6K	Cell Signaling Technology	Cat#9234S; RRID: AB_2269803
Rabbit polyclonal anti-VGAT	Merck Millipore	Cat#AB5062P; RRID: AB_2301998
Rabbit polyclonal anti-Neuroligin 2	Synaptic Systems	Cat#129 203; RRID: AB_993014
Rabbit anti-SLC7A5	Matsuo et al., 2000	N/A
Rat monoclonal anti-MECA32	Novus Biologicals	Cat#NB100-77668; RRID: AB_1084448
Rabbit polyclonal anti-Parvalbumin	Abcam	Cat#ab11427; RRID: AB_298032
Rat monoclonal anti-Ctip2	Abcam	Cat#ab18465; RRID: AB_2064130
Rabbit monoclonal anti-Cux1	Santa Cruz Biotechnology	Cat# sc13024
Rabbit polyclonal anti-Somatostatin-14	Penlabs Laboratories International	Cat#T-4103; RRID: AB_518614
Rabbit polyclonal anti-Calretinin	Swant	Cat#7697; RRID: AB_2619710
Chemicals, Peptides, and Recombinant Proteins		
RNasin Plus RNase Inhibitor	Promega	Cat#: N2611
SUPERase IN RNase inhibitor	Thermo Fisher Scientific	Cat#: AM2694
Critical Commercial Assays		
RNA 6000 Nano kit	Agilent	Cat#: 5067-1511
SENSE mRNA-Seq Library Prep Kit V2	Lexogen	N/A
High Sensitivity DNA Analysis Kit	Agilent	Cat#: 5067-4626
ALZET Mini osmotic pump model 1007D	ALZET	Cat#: 0000290
ALZET Mini osmotic pump model 2002	ALZET	Cat#: 0000296
ALZET Brain Infusion Kit 3	ALZET	Cat#: 0008851
Deposited Data		
Raw and analyzed data (Slc7a5)	This paper	GEO: GSE87808
Raw and analyzed data (Bckdk)	Novarino et al., 2012	GEO: GSE39447
Whole exome sequencing raw data (*SLC7A5*)	Novarino et al., 2012	NCBI: SRS351252
Experimental Models: Cell Lines		
Human: primary skin fibroblasts	This paper	N/A
Experimental Models: Organisms/Strains		
E. coli: strain Rosetta(DE3)pLysS	Galluccio et al., 2013	N/A
Mouse: *Slc7a5*$^{fl/fl}$ in pure *C57BL/6J* genetic background	Peter M. Taylor	N/A
Mouse: *Bckdk* $^{(OST79912)}$	Lexicon Pharmaceuticals	N/A
Mouse: Gt(ROSA)26Sor$^{tm4(ACTB-tdTomato,-EGFP)Luo}$/J	Jackson Lab	Cat#: 007576

(*Continued on next page*)

Continued		
REAGENT or RESOURCE	SOURCE	IDENTIFIER
Mouse: B6.Cg-Tg(Tek-cre)12Flv/J	Jackson Lab	Cat#: 004128
Recombinant DNA		
pH6EX3-wt SLC7A5	Galluccio et al., 2013	N/A
Sequence-Based Reagents		
Mutagenesis primer sequences	See Table S4	N/A
Software and Algorithms		
Origin 7	OriginLab Inc.	http://originlab.com
pCLAMP 10.4	Molecular Devices	https://www.moleculardevices.com/systems/conventional-patch-clamp/pclamp-10-software
FASTX toolkit 0.0.13.2	Hannon Lab	http://hannonlab.cshl.edu/fastx_toolkit/index.html
STAR 2.5.4	Dobin et al., 2013	https://github.com/alexdobin/STAR
R 2.3.4		https://www.r-project.org/
DESeq2 1.10.1	Love et al., 2014	http://bioconductor.org/packages/release/bioc/html/DESeq2.html
GOStats 2.36.0	Falcon and Gentleman, 2007	http://bioconductor.org/packages/release/bioc/html/DESeq2.html
Homozygosity Mapper	Seelow et al., 2009	http://www.homozygositymapper.org
Genome Analysis ToolKit (GATK1.1)	DePristo et al., 2011	https://software.broadinstitute.org/gatk/
SAMtools		http://samtools.sourceforge.net
Primer3		http://bioinfo.ut.ee/primer3/
Sequencher 4.9	Gene Codes Corporation	http://www.genecodes.com
GraFit (version 5.0.13)	Erithacus Software	http://www.erithacus.com/grafit/
ATLAS 5 array tomography	Zeiss	http://www.zeiss.com/microscopy/int/products/scanning-electron-microscopes/upgrades/atlas-5-array-tomography.html

CONTACT FOR REAGENT AND RESOURCE SHARING

Further information and requests for reagents may be directed to, and will be fulfilled by the lead author Gaia Novarino (gnovarino@ist.ac.at).

EXPERIMENTAL MODEL AND SUBJECT DETAILS

Mice

Experiments were performed in accordance with protocols approved by the Institutional Animal Care and Use Committee at IST Austria. Generation of the *Tie2*-Cre and *Slc7a5* floxed lines has been described previously (Kisanuki et al., 2001; Sinclair et al., 2013). For all experiments we made use of littermates derived from crossing Cre negative $Slc7a5^{fl/fl}$ females with Cre positive $Slc7a5^{fl/+}$ males. Mice were backcrossed to the N10 generation in C57BL/6J mice. Overall, $Tie2^{Cre}$;$Slc7a5^{fl/fl}$ transgenic animals were viable and fertile. Mice were housed together with their littermates in groups of 3-4 animals per cage and kept on a regular 12 hr light/dark cycle (7:00-19:00 light period). Food and water were available ad libitum. Experiments were carried out under pathogen-free conditions and health status of the mouse line was routinely checked by a veterinary. Experiments were carried out with randomly chosen littermates of the same sex. Both males and females were used with exception of the three-chamber test for which only males were employed. The genotype, age and developmental stage of the employed animals are specified separately for each experiment. For all the experiments the animals were drug and test naive but when possible mice were employed for different tests starting with the less aversive test (see behavioral study description).

Human Subjects and Sample Collection

Patients were identified from a cohort of over 2500 families, with at least one member of the family displaying a childhood onset neurological condition of likely genetic origin, from several world-wide recruitment efforts targeting patients with intellectual disability, structural brain diseases or neurodevelopmental disorders. Recruitment was focused in the major population centers of

the Middle East including Morocco, Libya, Egypt, Saudi Arabia, Kuwait, UAE, Oman, Jordan, Pakistan, Turkey and Iran, with consanguinity rates (i.e., rate of marriage between first or second cousins) of approximately 50% compared with < 1% is US and Western Europe. Among the recruited cohort, consanguinity was present in 63% of parents, suggesting some bias in sampling toward those with affected children due to recessive disease. Sampling was performed on both parents and all available genetically informative siblings to include affected and unaffected members, as well as extended family members if appropriate, consistent with IRB guidelines. All patients were evaluated directly by one of the co-authors with specialty training in neurology, child neurology and/or clinical genetics, and in accordance with local medical practices. All patients/families enrolled in IRB approved protocols based at referral institutions, and each family provided consent for study. Sequencing was performed on at least one but sometimes two affected or the father-mother-affected trio per family. Families 1426 and 1465 were identified and employed in this study because of comprising patients with homozygous disruptive mutations in the *SLC7A5* gene. Diagnosis of autism was set prior to whole exome sequencing and according to internationally accepted guidelines (DSM-V and CARS interview). Videos documenting the neurological examination and clinical features documentation were obtained in most of the cases.

Patient 1426-5 (female) was born at full term by normal delivery to a healthy mother after an uneventful pregnancy. There was no history of intellectual disability or epilepsy in the family. No chromosomal abnormalities were identified. Occipito-frontal head circumference (OFC) was −2 SD at birth and −5 SD in late childhood. The girl never learned to walk; she shows increased tone, clonus and dystonia since 5 years of age. She can bear some weight on the legs with support. She shows impaired social interaction, eye-to-eye gaze, and restrictive behaviors but has a social smile. She can understand simple commands but does not have speech. CARS (childhood autism rating scale) score at the age of 33 was 31 (autism cutoff 30). She has no seizures and she does not take any medication. She has no other health problems. There are no progressive features.

Patient 1426-6 (male), 1426-8 (female), 1426-16 (male) and 1426-19 (male) presentation and history are essentially similar to patient 1426-5. In late childhood all the patients present with various degrees of microcephaly (see Figure 5B). CARS score for patients 1426-6 and 1426-8 were 31 and 34 at the age of 17 and 12 years, respectively. Patient 1426-16 died of an unrelated cause during the preparation of this manuscript; therefore there is not updated information for this patient.

Importantly, all the affected individuals of family 1426 have normal plasma amino acid concentrations (Table S5).

Patient 1465-3 (male) was the second child, born to consanguineous parents (who were first cousins) at full term, after an uneventful pregnancy. He presented with intractable epilepsy and neurodevelopmental delay during his infancy period. The medical history of the family is notable for a previous case of microcephaly. The patient began walking at 48 months. Upon examination, his weight, height and head circumference measurements were under 3rd percent, he was hypotonic and microcephalic with slightly dysmorphic face. He was unable to speak. He had joint laxity in his lower extremities and pes planus in both feet.

Patient 1465-4 (male) has also been born at full term after a normal pregnancy, but displayed similar symptoms of abnormal development. Like his brother, he was brought to medical attention due to intractable seizures, which started when he was six months old. When he was 24-months-old he was able to sit without support. He never developed speech. At the time of examination, he was found to have microcephaly, hypotonia, slightly dysmorphic face, scoliosis, decreased subcutaneous fatty tissue and joint laxity in his hands and lower extremities. He was unable to speak or write, and was able to walk with support.

Cell Lines

Mutant and control fibroblasts were generated from explants of dermal biopsies following informed consent under protocols approved by the University of California San Diego or Yale University. Primary skin fibroblasts from affected and unaffected passage-matched controls were cultured in Dulbecco's Modified Eagle Medium supplemented with 10% fetal bovine serum and 1X Penicillin-Streptomycin. Cell lines were maintained in a 5% CO_2 incubator at 37°C. Cell lines were routinely tested to exclude *Mycoplasma* contaminations.

Protein Model

The SLC7A5 homology model was built based on the X-ray structure of the agmatine/arginine AdiC transporter from *E. Coli* in the outward-occluded arginine-bound conformation (PDB identifier 3L1L) (Gao et al., 2010). SLC7A5 and AdiC are members of the amino acid-polyamine-organocation (APC) transporter superfamily and exhibit sequence identity of about 22% (Geier et al., 2013; Saier et al., 2009). We used PyMOL to visualize the model and predict possible mutation effect on the protein structure (DeLano, 2002).

METHOD DETAILS

Amino Acid Analysis

Plasma Amino Acid Analysis in Mice

Adult mice were euthanized by cervical dislocation, decapitated and blood was collected (200 μL) from their trunks into commercially available anticoagulant treated tubes (e.g., heparin tubes Vacuette, Greiner Bio One). Cells were removed from plasma by centrifugation for 10 min at 2000 X g at 4°C. Following centrifugation the plasma supernatant was transferred into clean polypropylene tubes and kept at −70°C until assayed for amino acid concentrations by High Performance Liquid Chromatography (HPLC). Mouse plasma amino acid values reported in Table S1 represent mean ± SEM obtained from n = 4 mice per genotype.

Plasma Amino Acid Analysis in Humans

Patient blood samples were collected under fasting conditions. Blood samples were collected on Guthrie cards and analyzed by LC-MS/MS and flow injection analysis-tandem mass spectrometry (FIA-MS/MS) (Novarino et al., 2012). Plasma amino acid values reported in Table S5 are the result of a single blood amino acid test. Similarly, previous investigation didn't reveal serum amino acid levels abnormalities.

Brain Amino Acid Analysis in Mice

Adult mice were euthanized by cervical dislocation, decapitated and the left hemisphere of the brain was collected, weighed and immediately homogenized in 1 mL of ice-cold radio immunoprecipitation assay (RIPA) buffer (50mM Tris-HCl, pH = 7.4, 1% NP-40, 0.5% Na-deoxycholate, 0.1% SDS, 150 mM NaCl, 2 mM EDTA – all from Sigma-Aldrich) in the presence of cOmplete Protease Inhibitor Cocktail (Complete, Roche). The tissue was disrupted using a glass homogenizer, transferred into a collecting tube, and left on ice for 1 hr. The homogenate was centrifuged for 40 min at 100,000 X g at 4°C in a SW41Ti rotor in a Beckman Optima XPN-80 ultracentrifuge (Beckman Coulter), the supernatant was collected and deproteinized by the addition of an equal volume of a solution of 8% (wt/vol) 5-sulfosalicylic acid (Sigma-Aldrich) and stored at −70°C until assayed for amino acid concentrations. At the time of the assay, the samples were thawed, mixed, centrifuged for 30 min at 5,000 X g at 4°C to remove the precipitated protein and assessed by HPLC (performed at Archimedlife GmbH). Four to eight animals per genotype/per time point (E14.5, P2 and P40) were employed for determination of brain amino acid levels. HPLC analysis was performed blinded to genotype. Brain amino acid samples were tested in duplicate in 2 to 3 independent experiments except for the E14.5 for which all the samples were measured in duplicate but collected and measured at the same day.

RNA-Sequencing

Adult mice were euthanized under anesthesia and the brains were quickly dissected on ice. The cerebellum was used for RNA extraction by using 700 μL Trizol (Thermo Fisher Scientific) for homogenization and 140 μL chloroform (Sigma-Aldrich), followed by centrifugation at 12000 g for 15 min at 4°C. The upper aqueous phase was transferred to a new tube and 1.5 volumes of 100% ethanol were added. Total RNA was extracted by using the RNA Clean&Concentrator-5 prep Kit (Zymo Research). RQ1 RNase-Free DNase (Promega) treatment was also applied as described in the kit instructions manual. RNA sample quality was checked by using the NanoDrop spectrophotometer (Thermo Fisher Scientific) and the Bioanalyzer 2100 with the RNA 6000 Nano kit (Agilent). Then 1.5 μg total RNA was used to generate cDNA libraries by following the manufacturer's instructions in the SENSE mRNA-Seq Library Prep Kit V2 (Lexogen). Quality check of the generated libraries was assessed by using the Bioanalyzer 2100 with the High Sensitivity DNA Analysis Kit (Agilent). Libraries were sequenced on Illumina HiSeq 2500 instrument.

Western Blot

Adult mice were euthanized under anesthesia, the brain was dissected and homogenized in ice-cold RIPA buffer (50mM Tris-HCl, pH = 7.4, 1% NP-40, 0.5% Na-deoxycholate, 0.1% SDS, 150 mM NaCl, 2 mM EDTA – all from Sigma-Aldrich) supplemented with cOmplete Protease Inhibitor Cocktail (Complete, Roche) and/or with phosphatase inhibitor cocktail 3 (Sigma Aldrich). After 1 hr of incubation on ice, the lysates were centrifuged at 4°C at 14.000 g for 15 min. The protein concentration of the supernatant was measured using the BioRad protein assay method (BioRad). For the western blot, 30-50 μg proteins were mixed with Laemmli buffer 6x (375 mM Tris pH = 6.8, 12%SDS, 60% glycerol, 600 mM DTT, 0.06% bromphenol blue – all fro Sigma-Aldrich), heated to 95°C and then separated on 6%–15% SDS-PAGE gels in running buffer (3.03 g Tris base, 14.1 g glycine, 1 g SDS –Sigma-Aldrich, 1 L MilliQ water). Proteins were transferred to a nitrocellulose membrane using a transfer buffer (3.03 g Tris base, 14.1 g glycine, 1 L MilliQ water) for 2 hr at 4°C in a Bio-Rad Micro Cell western blotting apparatus (300 mA constant intensity). The membranes were blocked for 1 hr with 5% milk in 1x TBS with 1% Tween (TBST) and incubated with primary antibody overnight at 4°C. After 4x10 min washes with TBST, the membranes were incubated with the secondary antibody for 1 hr at room temperature. Horseradish peroxidase coupled anti-igG antibody was detected using an enhanced chemiluminescence substrate: Pierce ECL kit/Super Signal West Pico kit/Super Signal West Femto Maximum Sensitivity Substrate (Thermo Fisher Scientific). The following primary antibodies were used: rabbit anti-4E-BP1 (1:1000, Cell Signaling, 9644); rabbit anti-phospho-4E-BP1(1:1000, Cell Signaling, 2855); rabbit anti-eIF4E (1:1000, Cell Signaling, 2067); rabbit anti-phospho-eIF4E (1:1000, Cell Signaling, 9741); rabbit anti-eIF2 alpha (1:1000, Cell Signaling, 9722); rabbit anti-phospho-eIF2 alpha (1:1000, Cell Signaling, 3398); rabbit anti-S6K (1:1000, Cell Signaling, 2708); rabbit anti-phspho-S6K (1:1000, Cell Signaling, 9234); rabbit anti-VGAT (1:200, Millipore, AB5062P); mouse anti-Tubulin beta 3 (1:1000, BioLegend, MMS-435P). Secondary antibodies: donkey anti-rabbit HRP (1:1000, Thermo Scientific, A16035); goat anti-mouse HRP (1:1000, Thermo Scientific, 31432). Each western blot was repeated at least in 2 independent experiments.

Polysome Profiling

Adult mice were euthanized by cortical dislocation, dissected and the brains were removed. Cortices were separated and lysed in Lysis Buffer (20 mM HEPES pH 7.4, 150 mM KCl, 5 mM MgCl2, 0,5 mM DTT, 100 μg/mL cycloheximide- Sigma-Aldrich, Roche Complete Protease Inhibitors (EDTA-free), 40 U/mL RNAsin - Promega, 20 U/mL Superasin – Thermo Fischer Scientific) using a dounce. Lysates were centrifuged for 10 min at 2000 x g at 4°C and the resulting supernatants were supplemented with NP-40 and Triton X-100 (both to 1%) and incubated on ice for 5 min. After centrifugation for 10 min at 20000 x g at 4°C the debris-free supernatants were flash-frozen and stored at −80°C until further use. Thawed supernatants were loaded onto 14 × 95 mm Polyclear centrifuge

tubes (Seton) containing 17.5%–50% sucrose gradients (in Gradient Buffer containing 20 mM Tris-HCl pH 7.4, 5 mM MgCl2, 150 mM NaCl, 1 mM DTT, 100 μg/mL cycloheximide); the sucrose gradients were generated using the Gradient Master 108 programmable gradient pourer (Biocomp) and were centrifuged for 2.5 hr at 35,000 rpm in a SW40Ti rotor in a Beckman L7 ultracentrifuge (Beckman Coulter). After centrifugation gradients were fractionated and measured for RNA content using a Piston Gradient Fractionator (Biocomp) attached to a UV monitor (BioRad). Data represents mean ± SEM obtained from n = 9 KO and 10 WT mice from N = 2 independent experiments.

Immunohistochemistry

Adult mice were anesthetized by intraperitoneal injection (i.p.) of Ketamin 100mg/kg, Xylazine 10mg/kg and Acepromazin 3mg/kg as a mixture in one syringe. Unconscious state of the mouse was verified by pinching the hind limb (interdigital reflex). The diaphragm was opened from the abdominal side to expose the heart. A small incision was made in the right atrium and a butterfly needle was placed in the left ventricle to infuse phosphate buffered saline (PBS – Sigma-Aldrich) solution (25 mM Phosphate Buffer (PB), 0.9% NaCl) at 7 ml/min for 2 min using a perfusion pump. Afterward the PBS was exchanged with a fixative solution consisting of 4% Paraformaldehyde (PFA- Sigma-Aldrich) + 0.05% Glutaraldehyde (Sigma-Aldrich) solution in 0.1M PB (5-10 min). The brains were removed and post-fixed overnight in 4% PFA at 4°C. Next, brains were cryoprotected in 30% sucrose solution at 4°C for one day and embedded in Optimum Cutting Temperature (O.C.T., Tissue Tek) or removed from the sucrose and kept on dry ice and sliced. Free-floating 20 μm sections were cut using either a Microm HM560 cryostat (Thermo Fisher Scientific) or a sliding VT 1200S vibratome (Leica Microsystems). Cryostat sliced sections were used for stainings that required antigen retrieval (e.g., SLC7A5 staining) whereas the vibratome sliced sections were used for non-antigen retrieval staining and were collected in PBS. Slices were washed twice with PBS (10 min) at room temperature and then antigen retrieval was performed for 20 min at 98°C in Target Retrieval Solution (Dako) pH = 6 in an electric pot. Samples were cooled to room temperature and then washed again twice with PBS (10 min). The sections were permeabilized in 0.5% Triton X-100 in PBS for 30 min and then blocked for 40 min in 5% normal goat serum (Sigma-Aldrich) in 0.5% Triton X-100 in PBS at room temperature. Sections were then incubated overnight with primary antibody at 4°C. The sections were washed (3x10 min) with 0.01% Triton X-100 in PBS and incubated with secondary antibody for 1 hr at room temperature in a dark place. Sections were incubated with DAPI (10 min) and then washed (3x10 min) with 0.01% Triton X-100 in PBS and mounted onto glass slides with Mowiol (Sigma-Aldrich). Fluorescent signal was detected using a LSM 700 inverted confocal microscope (Zeiss). The following primary antibodies were used: rabbit anti-SLC7A5 (1:200, received from Prof. Kanai (Matsuo et al., 2000)); rat anti-MECA32 (1:600, Novus Biologicals, NB100-77668); rabbit anti-Parvalbumin (1:500, Abcam, ab11427); rat anti-Ctip2 (1:400, Abcam, ab18465); rabbit anti-Cux1 (1:400, Santa Cruz, sc13024); rabbit anti-Somatostatin (1:1000, Penlabs, T-4103); rabbit anti-Calretinin (1:4500, Swant, 7697); rabbit anti-VGAT (1:200, Millipore, AB5062P); rabbit anti-Neuroligin 2 (1:500, Synaptic System, 129203). The secondary antibodies used were: donkey anti-rabbit (1:1000, Alexa Fluor 488, Life Technologies, A-21206); goat anti-rat (1:1000, Alexa Fluor 647, Life Technologies, A-21247). Immunohistochemistry experiments were repeated in at least 3 independent experiments.

Nissl Staining

Adult mice were anesthetized and perfused with PFA 4% as described in the immunohistochemistry section. The brains were removed and post-fixed for 2 hr in 4% PFA at 4°C. Next, brains were transferred to 70% ethanol overnight at 4°C. The next day the ethanol was replaced with fresh 70% ethanol for another hour at room temperature, followed by 90% ethanol for 3 hr at room temperature and eventually 100% ethanol overnight at room temperature. On the following day brains were placed in a 1:1 mix of 100% ethanol: paraffin solution (ethanol is added from time to time to avoid complete evaporation) for 12 hr at 65°C and then moved to paraffin overnight at 65°C in an incubator. After this step brains were left to solidify in paraffin blocks and then 10 μm sections were cut on a HM 355S Microtome (Thermo Fisher Scientific). Paraffin slices were cleared with warm Roti-Histol (Carl Roth) for 10 min and passed through absolute ethanol to water (96%, 90%, 70%, 50%, 30%, water) each step for 5 min. Slices were then kept in 1% Cresyl Violet acetate (Thermo Fisher Scientific) solution for 4 min, followed by destaining solution (100 mL ethanol with 2 mL 100% acetic acid) for 5-10 s, absolute ethanol for 30 s and final absolute ethanol for 1 min. At the end slices were cleared with Roti-Histol (10 min) and mounted with DPX (Sigma-Aldrich). Images were acquired using the BX53 upright light microscope with an attached DP70 digital camera (Olympus) and processed with Photoshop CS5.1 (Adobe Systems). Nissl staining observation was repeated with 3 mice per genotype at two different developmental stages.

Electrophysiology

Littermates of the same sex but different genotypes were randomly used to prepare brain slices. Acute sagittal slices (300 μm) were prepared from the cortex and from the cerebellum of 19 to 22 days old mice (here referred as P21). Animals were anesthetized by an i.p. injection of a mixture of ketamin (100 mg/kg), xylazin (10 mg/kg) and acepromazin (3 mg/kg), then transcardially perfused with ice-cold carbogenated solution containing (mM): 64 NaCl, 25 NaHCO3, 2.5 KCl, 1.25 NaH2PO4, 10 glucose, 120 sucrose, 7 MgCl2 and 0.5 CaCl2 (all from Sigma-Aldrich, unless otherwise stated). After decapitation, brains were removed for sectioning in the same ice-cold cutting solution using a VT 1200S vibratome (Leica Microsystems). Slices were recovered in room-temperature carbogenated regular artificial cerebrospinal fluid (mM): 125 NaCl, 2.5 KCl, 1.25 NaH2PO4, 25 NaHCO3, 25 glucose, 1 MgCl2 and 2 CaCl2 (~320 mOsm, 7.2–7.4 pH) for 30 min and transferred to a recording chamber (RC-41LP, Warner Instruments) for experiments

typically between 1 and 7 hr after slicing. Slices were visualized under infrared-differential interference contrast (IR-DIC) using a BX-51WI microscope (Olympus) with a QIClickTM charge-coupled device camera (Q Imaging Inc, Surrey). Cerebellar Purkinje cells and cortical layer 2-3 pyramidal cells with a prominent apical dendrite were visually identified with a microscope equipped with IR-DIC optics mainly by location, shape and Clampex online membrane test parameters.

Borosilicate glass recording microelectrodes (World Precision Instruments) were pulled on a P-1000 horizontal puller (Sutter Instruments) and backfilled with an internal solution containing (mM): 115 cessium methanesulphonate, 8 NaCl, 10 HEPES, 0.3 EGTA, 10 Cs4BAPTA, 5 lidocaine N-ethyl chloride, 4 MgATP, 0.3 NaGTP, and 0.2% biocytin. Internal pH was adjusted to ~7.3 with CsOH and osmolarity adjusted to ~295 mOsm with sucrose. Typical internal resistance was around 1.7–3.5 MΩ. After seal rupture and internal equilibrium (5 min to allow proper dialysis of Cs+ internally), cells were recorded with series-resistance values < 10 MΩ (recording traces were excluded for data analysis if series resistance changed by > 25%). Slices were perfused with room temperature carbogenated regular aCSF at a rate of approximately 2 ml/min−1. Miniature excitatory postsynaptic currents (mEPSCs) were recorded at a holding potential of –70 mV and miniature inhibitory postsynaptic currents (mIPSC) at the reversal potential for mEPSC (+ 10 mV). All voltage clamp traces were recorded in the presence of 1 μM tetrodotoxin (Bio Trend) with theoretical liquid junction potential not corrected for. Signals were filtered at 0.1 kHz, digitized at 10 kHz and data acquired using a MultiClamp 700B amplifier and a Digidata 1550A.

Electron Microscopy

21 days old mice were anesthetized by i.p. injection of Ketamin 100mg/kg, Xylazine 10mg/kg and Acepromazin 3mg/kg as a mixture in one syringe. Unconscious state of the mouse was verified by pinching the hind limb (interdigital reflex). The diaphragm was opened from the abdominal side to expose the heart. A small incision was made in the right atrium and a butterfly needle was placed in the left ventricle to infuse PBS at 7 ml/min for 2 min using a perfusion pump. Afterward the PBS was exchanged with a fixative solution containing 4% PFA + 5% Glutaraldehyde in 0.1M PB (5-10 min). The brains were removed and post-fixed overnight in a 0.4% PFA in 0.1M PB at 4°C. 70 μm sections were cut using a Vibroslicer (Leica Microsystems), collected in PB and stored in PB+0.02% NaN_3. Sections were washed in PB and osmified with 2% osmium (Agar Scientific Ltd) in 0.1M PB for 45 min at room temperature. They were then washed in 0.1M PB (10 min) and distilled water (3x10 min), and contrasted with 0.1% uranylacetate (Agar Scientific) in 50% ethanol solution for 30 min at room temperature in the dark. Samples were washed in distilled water (3x10 min) and dehydrated in ascending ethanol solutions (50%, 70%, 90%, 96% and 100% for 10 min each), infiltrated in propylene oxide (2x10 min) and embedded in Durcupan ACM (Sigma-Aldrich): propylene oxide mix 1/2 for 1h at room temperature, 2/1 for 1h at room temperature and mere Durcupan overnight at room temperature. Samples were mounted on siliconized coverslips, placed on a heating plate for 30 min at 37°C and put in an oven for 2 days at 60°C to polymerize resin. The region of interest (layer 2/3 somatosensory cortex) was cut and re-embedded in a resin block for further slicing. 70 nm ultrathin serial sections were cut using an UC7 ultramicrotom (Leica Microsytems), collected on formvar-coated copper-slot grids and examined in FE-SEM. Merlin VP Compact with STEM detector (Zeiss).

Behavioral Studies

All behavioral studies were carried out during the light period. Mice were habituated to the test room for at least 1 hr before each test. In order to recover, mice were given one day between tests. All behavior apparatuses were cleaned between each trial with 70% ethanol. All behavioral tests were performed starting with the least aversive task first and ending with the most aversive. Behavioral tests were performed with P55 to P65 mice except for the juvenile social interaction test for which P25 to P35 animals were employed and the ultrasonic vocalization test for which P2 to P10 pups were used. Data are presented as mean ± SEM.

Open Field Test

Exploratory behavior in a novel environment was assessed by a 20 min session in an open field chamber (45cmL x 45cmW x30cmH) made out of gray Plexiglas. The animal was placed in the center of the arena and then recording was started. Locomotor activity (distance traveled and velocity) in the center/periphery of the arena as well as rearing were recorded by using a video camera and analyzed using the EthoVision XT 11.5 software (Noldus).

Three Chamber Test

Mice were tested for sociability as described previously (Moy et al., 2007). Specifically, the testing apparatus was a rectangular clear Plexiglas three chambers box (60cm (L) x 40cm (W) x 20 cm (H)). The dividing walls had doorways allowing access to each chamber. Age and sex matched animals were used for all tests. C57BL/6J mice were used as stranger mice and were habituated to placement inside the wire cage. Each test animal was first placed into the center chamber with open access to both left and right chamber, each chamber containing an empty round wire cage. The wire cage (12cmH, 11cm diameter) allows nose contact between mice but prevents fighting. After 10 min of habituation, during the social phase, an age-matched stranger was placed in the left chamber while a novel object was placed into the right chamber. The test animal was allowed to freely explore the social apparatus for 10 min and show whether it prefers to interact with the novel object or with the stranger mouse. At the end of the first 10 min, each mouse was tested in a second 10 min session to evaluate the preference for a novel stranger, which was placed inside the right wire cage. Number of nose contacts (< 5cm proximity) with the caged mouse was calculated.

Juvenile Social Interaction

Juvenile social interactions were assessed in 25-35 days old mice in the Noldus PhenoTyper 3000 Observer chamber (30cm (L) x 30cm (W) x 35 cm (H)) as previously described (Silverman et al., 2011). Prior to the interaction session mice were individually housed

for 1 hr. Two animals were placed simultaneously in the chamber and then recording started. Three types of interactions were assessed: wild-type/knockout; wild-type/wild-type and knockout/knockout, between age and sex matched subjects. Interactions were tracked for 10 min using a digital camera incorporated in the PhenoTyper chamber. Ineractions were scored using the EthoVision XT 11.5 software (Noldus) and included number of nose-nose sniffing and distance between subjects.

Walking Beam Test

Fine motor coordination and balance was assessed by the beam walking assay (Carter et al., 2001). This test essentially examines the ability of the animals to remain upright and to walk on an elevated and relatively narrow beam. The beam apparatus consists of several 1 m-long beams with diameters of 5 cm, 3 cm and 1 cm, resting 50 cm above the floor on two poles. During the test a mouse is placed on one extremity of the beam and a black box was placed at the end of the beam as finish point. The test took place over 3 consecutive days, 2 days training and 1 day testing (3 trials per day). In between trials mice were allowed to rest in their cages for 10 min. On the training days mice were allowed to cross the 5 and 3 cm beams while on the test day mice walked on the 1 cm beam. A nylon hammock was stretched below the beam to cushion any falls. A video camera was set on a tripod to record the performance. Performance on the beam was quantified by measuring the latency to cross the beam.

Isolation-Induced Ultrasonic Vocalizations (USVs) in Mouse Pups

Whistle like sounds (between 30-90 kHz) were recorded from newborn pups as previously described (Scattoni et al., 2009). A microphone (part of the Noldus UltraVox XT system) was placed inside a dark, soundproof polycarbonate box (37cm (L) x 37cm (W) x 57cm (H)). Neonatal pups (postnatal days 2, 4, 6, 8, 10) were separated from their mother and placed inside the recording chamber. USVs were recorded for 3 min and afterward the pup was placed back with its mother until weaning time.

Gait Measurement Test

Gait was analyzed by performing the footprint test as previously described (Carter et al., 2001). Specifically, the fore and hind paws were painted with nontoxic dyes of different colors and then the mouse was allowed to walk in a straight line (in a narrow corridor using as bait a cage at the end of the walkway) over absorbent paper. The footprint patterns were then analyzed for stride length, sway length and stance length.

Marble Burying Test

Stereotyped behavior was assessed by placing adult mice (60 days old) into an usual animal cage (30cm (L) x 20cm (W) x 20cm (H), Tecniplast) filled with 5cm deep chip bedding, as previously described (Deacon, 2006). Bedding was reused between sex matched animals. A regular pattern of glass marbles (5 rows of 4 marbles) was placed on the bedding and the subject was allowed to explore for 25 min. The number of buried (to 2/3 of their depth in bedding) marbles was counted.

Hind Limb Clasping Test

As previously described (Guyenet et al., 2010), mice were grasped by their tail and suspended. Hind limb position was observed for 10 s. If the hind limbs were retracted toward the abdomen then the mouse was marked as positive for clasping. The test was repeated three times. At the end of the test the mouse was placed back into its cage. The test was repeated three times for each animal.

Kyphosis Test

Kyphosis is a characteristic curvature of the spine that is common in mouse models of certain neurological disorders (Guyenet et al., 2010). The mouse was removed form its cage and placed on a flat surface. While it was walking, we observed whether it was able to easily straighten its spine completely. If it was not the case, the mouse was marked as positive for kyphosis. At the end of the test the mouse was placed back into its cage. The test was repeated three times for each animal.

Intracerebroventricular Dye Injection

40 days old mice were injected s.c. with meloxicam 5 mg/kg one hour prior surgery in order to achieve analgesia and then anesthetized initially with isoflurane 4% and O2 0.5-1L/min in a gas chamber. Once anesthetized (checked by toe pinching), the mouse was placed in a Kopf stereotaxic frame and a nose cone was placed over the nose with isoflurane volume turned down to 2% to maintain the anesthesia. After sterilizing the surgical site with betadine, a midline incision was made over the skull and a small hole was drilled above the left lateral ventricle. Using a Hamilton syringe, connected to the Kopf stereotactic frame, 10 μL of dye was delivered into the ventricle in order to check later on the injection site accuracy. The coordinates used relative to bregma were: anterioposterior (AP) = −0.5 mm, medial lateral (ML) = −1.1 mm, dorsal ventral (DV) = −3 mm. To allow diffusion of the dye into the brain, the needle was left for 5 min at the site of injection. The incision was manually closed using a topical tissue adhesive (GLUture, World Precision Instruments). Two hours later the mouse was euthanized and the brain was kept overnight in 4% PFA. The next day the brain was embedded in 3% agarose blocks and then sliced (100 μm) using a VT 1200S vibratome (Leica Microsystems) in order to assess the diffusion of the dye in the entire ventricular system and to confirm the correct positioning of the needle in the left ventricle.

Serial Surgical Implantation of Cannula and Osmotic Pumps

One day before the surgery, a micro-osmotic pump (ALZET model 1007D) was filled with 100 μL of a saline amino acid solution (isoleucine 100 mM, leucine 100 mM). The pump was then connected through a plastic catheter to a cannula with a 0.5 mm spacer attached to it (ALZET Brain Infusion Kit 3). The pump was designed to deliver the solution at a rate of 0.5 μL/hour for 7 days. The pump and cannula assembly was kept in saline overnight at 37°C. Adult mice were injected s.c. with meloxicam 5 mg/kg one hour prior surgery in order to achieve analgesia and then anesthetized initially with isoflurane 4% and O_2 0.5-1L/min in a gas chamber.

Once anesthetized (checked by toe pinching), the mouse was placed in a Kopf stereotaxic frame and a nose cone was placed over the nose with isoflurane volume turned down to 2% to maintain the anesthesia. Eyes were covered with ointment in order to prevent drying out. During surgery metamizol 200mg/kg was administered subcutaneously (s.c.) to ensure maintenance of analgesia. After sterilizing the surgical site with betadine, a midline incision was made over the skull and a subcutaneous pocket was created on the back of the animal. The pump was then inserted inside the pocket and a small hole was drilled above the left lateral ventricle following the coordinates identified during the calibration study performed with dye injections and as previously described (DeVos and Miller, 2013), AP = −0.5 mm, ML = −1.1 mm, DV = −2.5mm. The incision was manually closed using a topical tissue adhesive (GLUture, World Precision Instruments). The incision site was sterilized with betadine and an ointment was applied to keep the spot moisturized. One week later the pump was replaced with a 200 μL micro-osmotic pump (ALZET model 2002) filled with the same amino acid solution as mentioned above. The replacement procedure was done following the same steps as described for the 100 μL pump. The mice were singly caged until the time for behavioral testing (e.g., walking beam test, gait measurement, open field test). Behavioral tests were performed with P55 to P65 mice. At the end of the three-week administration, mice were euthanized and their brains were dissected for HPLC protein analysis. Data represent means ± SEM; n = 10 (untreated) control, n = 4 (treated) control, n = 11 (untreated) mutant and n = 8 (treated) mutant mice.

Whole Exome Sequencing, Homozygosity Profile, and Variant Prioritization

DNA was extracted from peripheral blood leukocytes using salt extraction. For family 1426 blocks of homozygosity were determined by HomozygosityMapper. Whole-Exome Sequencing and variant analysis was performed using solution hybrid SureSelect reagents (Agilent, Mountain View, CA) and sequenced on an Illumina GAIIx or HiSeq2000 instrument (Gnirke et al., 2009). The sequence reads were aligned to the human genome (hg19), genetic variants were delineated using the Genome Analysis ToolKit (GATK 1.1) software and SAMTools (v1.4-r985) algorithms, for both single nucleotide polymorphisms (SNPs) and Indels.

Variants were prioritized using the following criteria:

1. The variant was predicted to perturb protein function. All synonymous and intronic variants were excluded unless the variant was within a predicted splice site (+ or −2 bp from splice junction). Any variation that was predicted to alter gene expression or protein function was included. These included nonsynonymous variations in coding regions (i.e., missense) or alterations resulting in frameshifts, premature stop codons, loss of stop codons, coding INDELS, and splice sites (i.e., ± 2 nucleotides from an exon junction).
2. The variant was rare as defined by allele frequency of less than 0.2%. Allele frequencies were determined by an in-house database of over 1500 Middle Eastern exomes, and public databases provided by The Exome Variant Server from NHLBI GO Exome Sequencing Project (ESP) and dbSNP135.
3. The variant was present in a region of homozygosity as defined by HomozygosityMapper.
4. The variant was highly conserved throughout evolution as determined by a number of conservation scores including GERP, PhastCons, and PolyPhen2. Variations with negative GERP scores or vertebrate PhastCons scores less than 0.8 were excluded. Typical conservation criteria for the candidate genes provided in this study were GERP > 4 and vertebrate PhastCons > 0.9.
5. The variant segregated with the disease in the family pedigree. All variants following the above criteria were considered for each family independent of its predicted severity (i.e., no variants were excluded based upon type of mutation).

The remaining variants were ranked by type of mutation (indels > nonsense > missense), amino acid conservation across species and protein damage prediction based upon location of the mutation in a specialized protein domain. The variants were annotated for novelty and compared with dbSNP (build 132) and control samples analyzed by whole-exome sequencing experiments performed by our human genomics groups. Variants were analyzed against the RefSeq gene definitions, a list that includes 18,933 specific genes. Where multiple isoforms gave varying results the one most likely to lead to protein disruption was chosen.

Sanger Sequencing

Primers were designed using the Primer3 program and tested for specificity using ENSEMBL's BLAST software. PCR products were treated using Exonuclease I (Thermo Fisher Scientific) and Shrimp Alkaline Phosphatase (Affymetrix) and sequenced using the Big Dye terminator cycle sequencing Kit v.3.1 (Applied Biosystems) on an ABI 3100 DNA analyzer (Applied Biosystems). The sequence data were analyzed using Sequencher 4.9 (Gene Codes).

Leucine Uptake Assay

Leucine uptake was performed as previously described (Sinclair et al., 2013). Briefly, 300.000 cells were plated in a single well of 6 well plates two days before the assay. The day of the experiment the cells were washed twice with HBSS and incubated in HBSS containing [^{3}H] leucine (Perkin Elmer) 0.5 uCi/ml alone or in the presence of 10 mM leucine or 3 mM BCH (Wang et al., 2011). Cells were incubated at 37°C for 1 hr. At the end of the incubation each well was washed twice with cold PBS and lysed with 1 mM NaOH for 2 hr at 37°C. Total leucine uptake was measured by liquid scintillation counting (Packard Tri-Carb 2100TR).

Cloning, Mutagenesis, and Expression of the Human SLC7A5 Wild-Type and Mutants

The construct pH6EX3-wt SLC7A5 obtained as previously described (Galluccio et al., 2013) and containing the SLC7A5 cDNA was used for site-directed mutagenesis. Specific mutants of the SLC7A5 cDNA were obtained by PCR overlap extension methods, as previously done for other proteins (Galluccio et al., 2015), using the primers in Table S4.

To supply tRNA for rare codons, Rosetta(DE3)pLysS *E. coli* strain was transformed either with SLC7A5 wild-type or mutant proteins (Galluccio et al., 2013) and selected on agar plates supplemented with ampicillin and chloramphenicol. A colony was picked and cultured overnight at 37°C under rotary shaking (about 200 rpm) in selective LB broth and the day after was diluted 1:10 in same medium. When the culture reached the mid logarithmic phase of growth, 0.4 mM IPTG was added and temperature was lowered at 28°C for 4 hr as previously described (Galluccio et al., 2013).

Purification of Human SLC7A5 Wild-Type and Mutants

Pellets from induced cell lysates were used for protein purification as previously described (Napolitano et al., 2015). In brief, after washing (0.1 M Tris HCl pH 8.0), pellets were solubilized using a 20 mM Tris/HCl pH 8.0 buffer containing 10 mM DTE, 0.8% sarkosyl, 3.5 M urea, 10% glycerol, 200 mM NaCl. Solubilized cell lysates were centrifuged (12,000 g, 10 min, 4°C) and the supernatants were applied on a His Trap HP column (5 mL Ni Sepharose), connected to fast protein liquid chromatography (FPLC) ÄKTA start and equilibrated with 10 mL buffer (20 mM Tris HCl pH 8.0, 10% glycerol, 200 mM NaCl, 0.1% sarkosyl, and DTE 2 mM). During purification procedure, column was washed with 10 mL of washing buffer (20 mM Tris HCl pH 8, 10% glycerol, 200 mM NaCl, 0.1% n-Dodecyl β-D-maltoside and 3 mM DTE – all from Sigma-Aldrich). Then, proteins were eluted by an isocratic step of 400 mM imidazole in the above described buffer. Fractions 6-8 (2.5 mL) were pooled and desalted on a PD-10 column using a desalting buffer (20 mM Tris HCl pH 8.0, 10% glycerol, 0.05% n-Dodecyl β-D-maltoside and 10 mM DTE).

Reconstitution of Human SLC7A5 Wild-Type and Mutants in Proteoliposomes

The purified SLC7A5 wild-type and mutants were reconstituted by removing the detergent using the batch-wise method as previously described (Napolitano et al., 2015). In brief, 4 μg of protein (in 200 μL) were mixed to 100 μL of 10% C12E8, 100 μL of 10% egg yolk phospholipids (w/v) in the form of sonicated liposomes prepared as previously described (Scalise et al., 2014), 20 mM Tris HCl pH 7.5, 10 mM DTE, 100 mM K-gluconate and 10 mM l-His, except where differently indicated, in a final volume of 700 μL. The mixture was incubated with 0.5 g Amberlite XAD-4 resin under rotatory stirring (1200 rev/min) at room temperature (25°C) for 90 min (Napolitano et al., 2015).

Transport Measurements

After reconstitution uptake and efflux experiments were conducted at 25°C. For uptake experiments, 600 μL of proteoliposomes were passed through a Sephadex G-75 column (0.7 cm diameter × 15 cm height) pre-equilibrated with 20 mM Tris HCl pH 7.5 and sucrose at appropriate concentrations to balance the internal osmolarity. Transport was started by adding 5 μM [^{3}H]His to the proteoliposomes. For efflux experiments, proteoliposomes containing 2 mM His, were preloaded with 5 μM [^{3}H]His at high specific radioactivity (1 μCi/ml) for 30 min by transporter-mediated exchange equilibration. Proteoliposomes were then passed through Sephadex G-75, as above described, to remove external compounds. Efflux was started by adding, or not, 1 mM of unradiolabelled His. In both uptake and efflux assays, transport was stopped by adding a mix of 10 μM 2-amino-2-norbornanecarboxylic acid (BCH) and 1 μM $HgCl_2$ at the desired time interval. In control samples, the inhibitor was added at time zero. At the end of the transport assay, each sample of proteoliposomes (100 μL) was passed through a Sephadex G-75 column (0.6 cm diameter × 8 cm height) to separate the external from the internal radioactivity. Proteoliposomes were eluted with 1 mL 50 mM NaCl and collected in 4 mL of scintillation mixture, vortexed and counted. The experimental values were corrected by subtracting each sample inhibited at time zero. For kinetic measurements, the initial rate of transport was measured by stopping the reaction after 10 min, i.e., within the initial linear range of [^{3}H]His uptake.

Ultracentrifugation of Proteoliposomes

SLC7A5 WT and SLC7A5-A246V reconstituted proteoliposomes were passed through Sephadex G-75 column and 500 μl were ultracentrifuged (110,000 g, 1 hr 30 min, 4°C). Pellets were washed with 20 mM Tris HCl pH 8.0 and ultracentrifuged again. Pellets were solubilized with 3% SDS and subjected to SDS-PAGE 12% run and western blot analysis. SLC7A5 WT and mutants were immunodetected using anti-SLC7A5 antibody 1:2000, upon overnight incubation at 4°C. The reaction was detected by Electro Chemi Luminescence (ECL) assay after incubation with secondary antibody anti-rabbit 1:5000.

QUANTIFICATION AND STATISTICAL ANALYSIS

Statistical values including the exact *n,* statistical significance, definition of center, and dispersion and precision measures are reported in the Figure Legends. Student's t test was mostly used and one-way ANOVA was used where appropriate (i.e., multiple comparisons). Data are shown as means ± SEM and were judged to be statistically significant when $p < 0.05$. In each graph circles/dots represent individual values. All datasets were analyzed using Shapiro–Wilk test for normality.

Amino Acid Data

Amino acid levels were normalized on the initial protein concentration and are displayed as fold change (log2 transformed) to levels in controls. Data analysis was done in GraphPad Prism 7 and Student's t test was used to test for significance. Mouse plasma amino acid values reported in Table S1 represent mean ± SEM obtained from n = 4 mice per genotype. Brain amino acid values represent mean ± SEM obtained from 4 to 8 mice per genotype per time point from at least 2 independent experiments.

RNA-Sequencing

Demultiplexed raw reads were trimmed before alignment as suggested by the library preparation kit, i.e., the first 9 bases of each read were removed using the FASTX toolkit. Trimmed reads were aligned to the mouse genome using STAR version 2.5.4 (genome: GrCm38, gene annotation: Gencode release M8). Reads that didn't align uniquely were discarded. Read counts per gene were also calculated using STAR (option -quantMode GeneCounts). Differential expression analysis was performed in R 3.2.4 employing the Bioconductor package DESeq2 version 1.10.1 using an FDR threshold of 0.05, a local fit for the dispersion estimation and default parameters otherwise. Gene Ontology enrichment analysis was done using the Bioconductor package GOstats version 2.36.0 with a p value cutoff of 0.001 and conditional testing enabled. GO enrichment results were visualized using a custom script. RNA sequencing was performed employing n = 3 mice per genotype.

Protein Data

Western Blot

Western blot images were acquired by Peqlab Fusion SL Advance Multi Imaging system (VWR) and quantified using ImageJ software. Protein levels are displayed as fold change. Student's t test was used to test for significance (GraphPad Prism 7). Data represent mean ± SEM obtained from two to five mice per genotype typically from at least 2 independent experiments.

Polysome Profiling

Analysis was performed blinded to genotype. For quantitative analysis of individual elements (e.g., 80S monosomes, polysomes, etc) from the polysome profiles, all traces were first exported to Microsoft Excel and adjusted as necessary to ensure matching x/y axis scales. Traces were then exported to Photoshop CS5.1 and ImageJ for processing, baseline setting, cropping and pixel counting. The pixel counts were used for determining polysome/monosome values and for plot generation. Student's t test was used for the statistical analysis (GraphPad Prism 7). Data represents mean ± SEM obtained from n = 9 KO and 10 WT mice from two independent experiments. All datasets were analyzed using Shapiro–Wilk test for normality.

Immunohistochemistry

Fluorescent signal was detected using a LSM 700 inverted confocal microscope (Zeiss) and images were processed with Photoshop CS5.1 (Adobe Systems). Control and mutant samples were always treated equally and in parallel (e.g., if brightness or contrast were adjusted identical changes were applied for all the samples). For each antibody, immunostainings were repeated in multiple animals (typically 3 per genotype) obtaining comparable results. We counted all parvalbumin, somatostatin and calretinin interneurons as well as VGAT and NLGN2 puncta intensity on coronal sections at different positions. Neurons/puncta quantified in a given animal were added together. Means and SEM were calculated across animals, and Student's t test was done across animals (n = 3 animals per genotype).

Neuronal Data

Analysis was performed blinded to genotype using pCLAMP 10.4 software (Axon Instruments/Molecular Devices). Statistical analyses were performed using Origin Software (Origin Inc), Clampfit and R. All datasets were analyzed using Shapiro–Wilk test for normality. Datasets with normal distributions were analyzed for significance using one-way ANOVA measures with Bonferroni post hoc test, using *$p < 0.05$, **$p < 0.005$. Datasets with non-normal distributions were analyzed using the 2-tailed Mann-Whitney U test using *$p < 0.05$. Exact P values are presented in each figure. Cumulative distributions were analyzed using the Kolmogorov-Smirnov test. Data represent means ± SEM, $n_{cells}/n_{animals}$/genotype: 14/7/*Tie2*^{Cre};*Slc7a5*$^{fl/+}$ and 13/5/*Tie2*^{Cre};*Slc7a5*$^{fl/fl}$ (mEPSC); 16/7/*Tie2*^{Cre};*Slc7a5*$^{fl/+}$ and 18/5/*Tie2*^{Cre};*Slc7a5*$^{fl/fl}$ (mIPSC).

Electron Microscopy

Analysis was performed blinded to the genotype. ATLAS 5 array tomography (Zeiss) was used for image acquisition and 3D reconstruction of sample data. ImageJ software was used for quantification of the symmetric synapse vesicular pool and measurement of the presynaptic terminal area. All datasets were analyzed using Shapiro–Wilk test for normality and met the criteria for normality. GraphPad Prism 7 was used for statistical analysis applying Student's t test. Data represent means ± SEM; $n_{synapses}$/genotype: 27/control and 22/mutant.

Behavior

Quantification of the different behavioral parameters was done using the EthoVision XT 11.5 (Noldus) and UltraVox XT software (Noldus). Data met the criteria for normal distribution (Shapiro–Wilk test), thus Student's t test was used for statistical analysis for most of the behavioral data. For the three chamber test one-way ANOVA with Fisher's post hoc test was applied and for the juvenile social interaction test one-way ANOVA with Bonferroni's post hoc test was used (GraphPad Prism 7). Number of animals employed

for each test is reported in the figure legend describing each experiments and range from n = 6 to n = 13 animal per genotype. At least two independent cohorts were examined for each test.

Transport Measurement Data

For the efflux experiments, the [^{3}H]His efflux was calculated by subtracting radioactivity values at each time point from that present in the proteoliposomes at time zero.

Uptake data were fitted in a first-order rate equation to obtain rate constants and in Michaelis–Menten or Linewever-Burk equations. Efflux data were fitted in a single exponential decay equation. The Grafit software (version 5.0.13) was used for data fitting. To measure the specific activity of SLC7A5 WT and mutants, protein quantity was estimated from Coomassie blue stained SDS-PAGE gels by using the Chemidoc imaging system equipped with Quantity One software (Bio-Rad) as previously described (Galluccio et al., 2012). Data represent mean ± SD obtained from n = 4 to 5 independent experiments.

For the fibroblast leucine uptake assay the results of were obtained from at least 3 independent experiments (5 for family 1426 and 3 for family 1465) each one employing fibroblasts from at least 1 unaffected and 1 affected individual of the same family. For family 1426, given the very invasive procedure, we obtained skin biopsies only from 2 affected (patient 1426-6 and 1426-19) and 2 unaffected individuals (1426-1 and 1426-2). The graph in Figure 6E represents the average of the transport values obtained for either both the affected or the unaffected subjects in all the performed experiments. As deducible from the small error bar we didn't notice strong variability among individuals of the same family.

DATA AND SOFTWARE AVAILABILITY

Data Resources

The accession numbers for the RNA-seq and microarray data reported in this paper are NCBI GEO: GSE87808 and GSE39447, respectively. The accession number for the whole exome sequencing data reported in this paper is NCBI SRA: SRS351252.

ADDITIONAL RESOURCES

The URLs for data presented herein are as follows:

Online Mendelian Inheritance in Man (OMIM): http://www.omim.org
SeattleSeq Annotation: http://gvs.gs.washington.edu/
Genome browser: http://www.genome.ucsc.edu/
HPLC analysis: http://www.archimedlife.com/de/

Cell

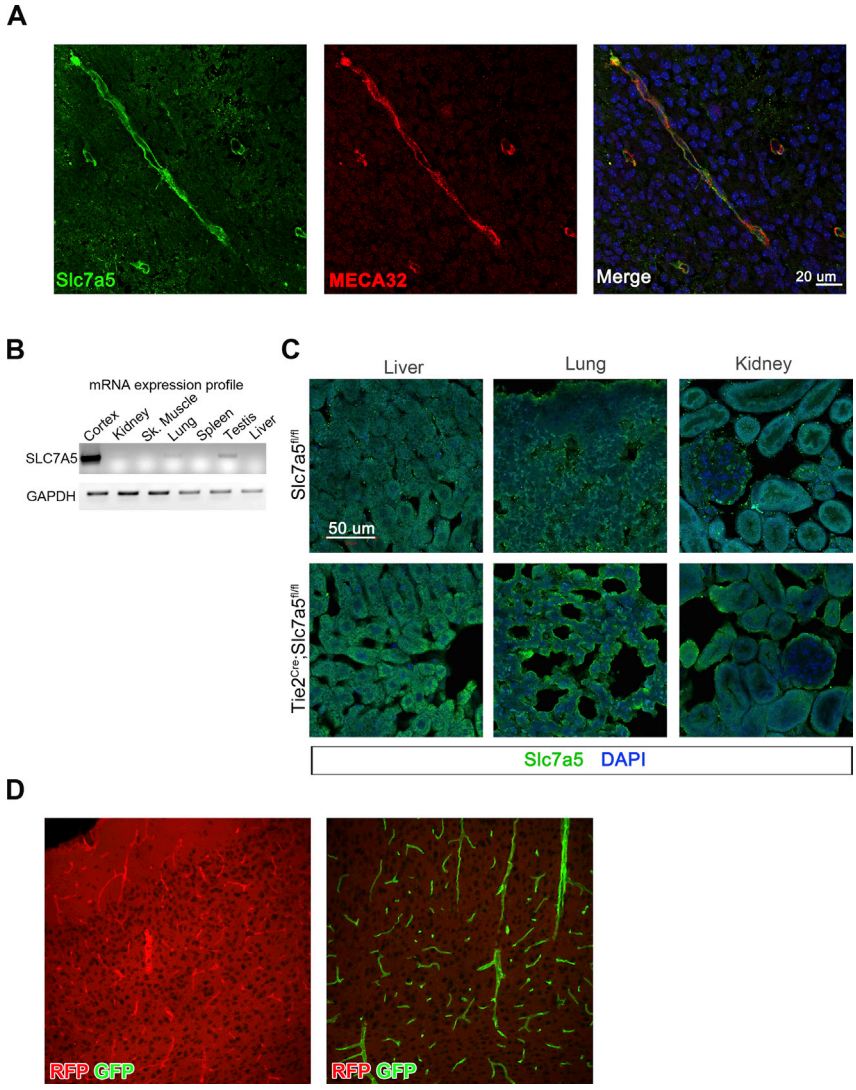

Figure S1. *Slc7a5* and *Tie2Cre* Expression at the BBB, Related to Figure 1

(A) Representative images of cortical slices stained with Slc7a5 (left) and the endothelial cell marker MECA 32 (middle) antibodies. The merged image (right) displays the co-localization of the two markers in control animals.

(B) Human mRNA expression profile in different tissues (top) reveals almost exclusive expression of SLC7A5 in the cortex. Sampled tissues are: cortex, kidney, skeletal muscle, lung, spleen, testis, liver. GAPDH (bottom) was used as internal control.

(C) Representative Slc7a5 (green) immunostained mouse tissue slices from control *Slc7a5*$^{fl/fl}$ (top) and mutant *Tie2*^{Cre}*Slc7a5*$^{fl/fl}$ (bottom) animals. Tissues were sampled from adult (> P40) mice and they include: liver (left), lung (middle) and kidney (right). Nuclei were stained with DAPI (blue).

(D) Tie2-driven Cre recombinase expression in the BBB was verified by crossing *Tie2*^{Cre} mice with the reporter line Gt26Sor. Gt26Sor mice express cell-membrane localized red fluorescencent protein (RFP) in widespread cells and tissues prior to Cre recombinase exposure and cell membrane-localized green fluorescencent protein (GFP) in Cre recombinase expressing cells. Note GFP staining in the endothelial cells of the BBB (right). Images were obtained from the cerebral cortex of 2 days old (P2) mice.

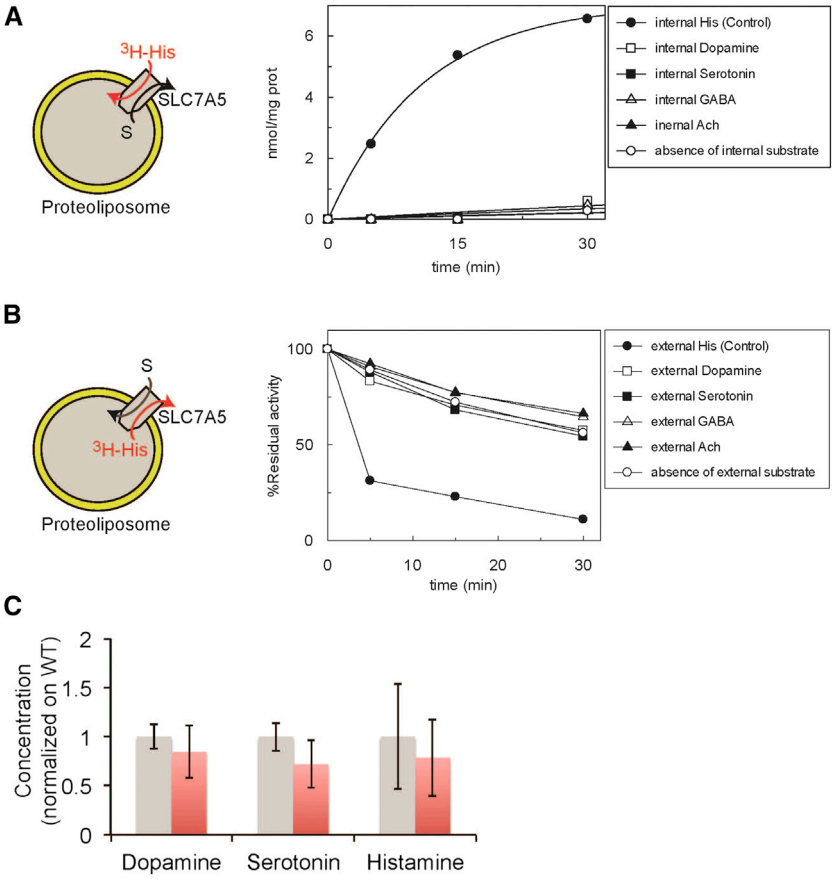

Figure S2. *Slc7a5* Does Not Transport Neurotransmitters, Related to Figure 1

(A and B) Left: Schematic of the in vitro transport assay - transport followed as uptake (A) of external [^{3}H]His in exchange to internal substrate (S) or as efflux (B) of internal [^{3}H]His in exchange with external substrate (S) in proteoliposomes with reconstituted SLC7A5 protein. Right: SLC7A5-mediated His uptake (A) and efflux (B) analysis indicates the inability of SLC7A5 to transport the tested neurotransmitters. Transport was started by adding 5 μM [^{3}H]His at time 0 to proteoliposomes containing 10 mM His, or the tested neurotransmitter, reconstituted with human SLC7A5 and stopped at the indicated times. Percentage of His efflux (B, % Residual activity) was calculated with respect to time 0 for each experimental condition. His-histidine; L-DOPA, L-3,4-dihydroxyphenylalanine; Ach-acethylcholine.

(C) Normal brain neurotransmitter levels in brain lysates of *Tie2^{Cre};Slc7a5$^{fl/fl}$* (red bars) mice. Neurotransmitter levels were quantified by HPLC and normalized on protein concentration and on control (*Tie2^{Cre};Slc7a5^{fl}/+,* gray bars) littermate levels (means ± SD; n = 4 mice per genotype).

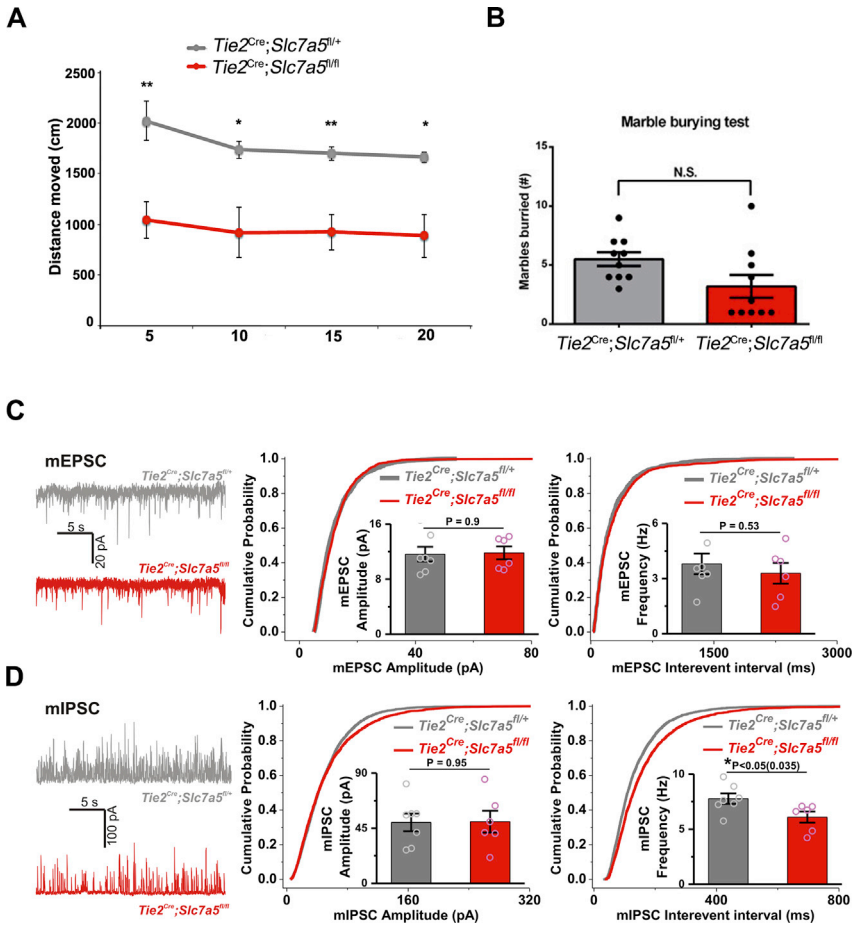

Figure S3. Behavioral and Electrophysiological Alterations in *Tie^{2Cre};Slc7a5$^{fl/fl}$* Mice, Related to Figures 3 and 4

(A) *Tie2^{Cre};Slc7a5$^{fl/fl}$* (red) and *Tie2^{Cre};Slc7a5$^{fl/+}$* (gray) show similar habituation kinetics in the open field. Distance moved in the open field was analyzed in 5 min bins over the course of 20 min. *Tie2^{Cre};Slc7a5$^{fl/fl}$* mice moved less at all given points *p < 0.05, **p < 0.01 (means ± SEM; n = 10 mice per genotype).

(B) Marble burying test shows no significant difference between the number of marbles buried by the control *Tie2^{Cre};Slc7a5$^{fl/+}$* and the mutant *Tie2^{Cre};Slc7a5$^{fl/fl}$*; N.S., not significant (means ± SEM; n = 10 mice per genotype; circles represent individual values).

(C and D) Left: Representative mEPSC (B) and mIPSC (C) recordings from *Tie2^{Cre};Slc7a5$^{fl/+}$* (gray) and *Tie2^{Cre};Slc7a5$^{fl/fl}$* (red) cerebellar Purkinje cells. Right: Cumulative probability distributions of peak amplitudes and interevent intervals of mEPSC (B) and mIPSC (C) in the two genotypes. Insets: quantifications of mean amplitudes and mean frequencies of the corresponding currents, along with absolute P values. Significant reduction in mIPSC mean frequency in mutants versus controls is indicated. Result confirmed by cumulative probability distribution analysis, Kolmogorov-Smirnov test: D = 0.109; *p < 0.05 (means ± SEM; n_{cells}/$n_{animals}$/genotype: 7/3/*Tie2^{Cre};Slc7a5$^{fl/+}$* and 6/3/*Tie^{2Cre};Slc7a5$^{fl/fl}$*; circles indicate individual values). mEPSCs and mIPSCs were recorded from the same cell.

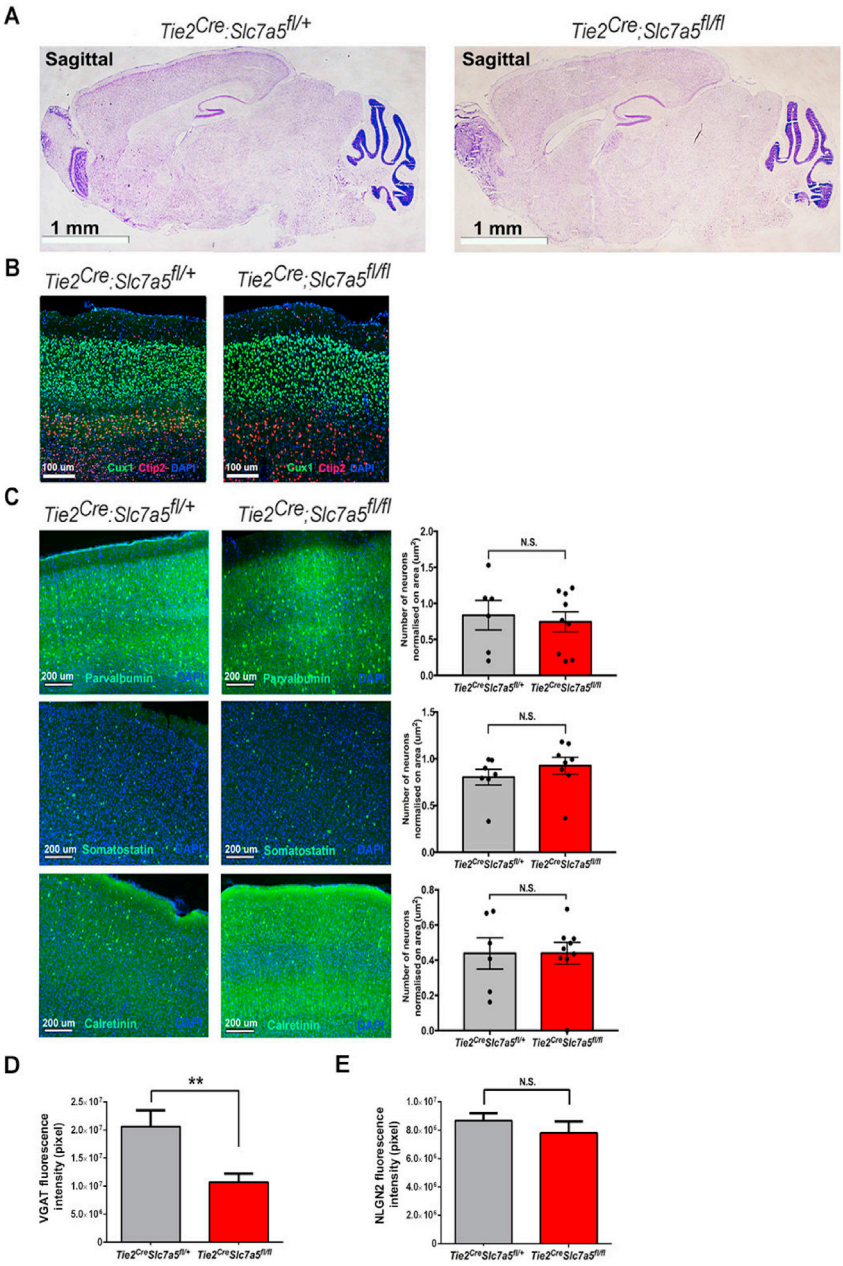

Figure S4. Absence of Gross Alterations in Brain Architecture of *Tie^{2Cre};Slc7a5$^{fl/fl}$* Mice, Related to Figure 4

(A) Nissl staining of sagittal sections of adult mouse brain indicating no differences in gross morphology between the control *Tie2^{Cre};Slc7a5$^{fl/+}$* and mutant *Tie2^{Cre};Slc7a5$^{fl/fl}$* mice.

(B) Immunostaining of Cux1 (green, upper layer neurons) and Ctip2 (red, lower layer neurons) shows similar cortical layer distribution in the two genotypes.

(C) Representative images (left) and quantifications (right) indicating similar numbers of parvalbumin- (top), somatostatin- (middle) and calretinin- (bottom) positive interneurons in the cortices of wild-type and mutant mice; N. S., not significant (means ± SEM; n = 3 mice per genotype; filled circles indicate individual values). Nuclei were stained with DAPI (blue).

(D) Fluorescence intensity quantification of VGAT puncta in control *Tie2^{Cre};Slc7a5$^{fl/+}$* compared to mutant *Tie2^{Cre};Slc7a5$^{fl/fl}$* mice; **p < 0.01 (means ± SEM; n = 3 mice per genotype).

(E) Fluorescence intensity quantification of NLGN2 puncta displaying no difference between control *Tie2^{Cre};Slc7a5$^{fl/+}$* and mutant *Tie2^{Cre};Slc7a5$^{fl/fl}$* mice; N.S., not significant (means ± SEM; n = 3 mice per genotype).

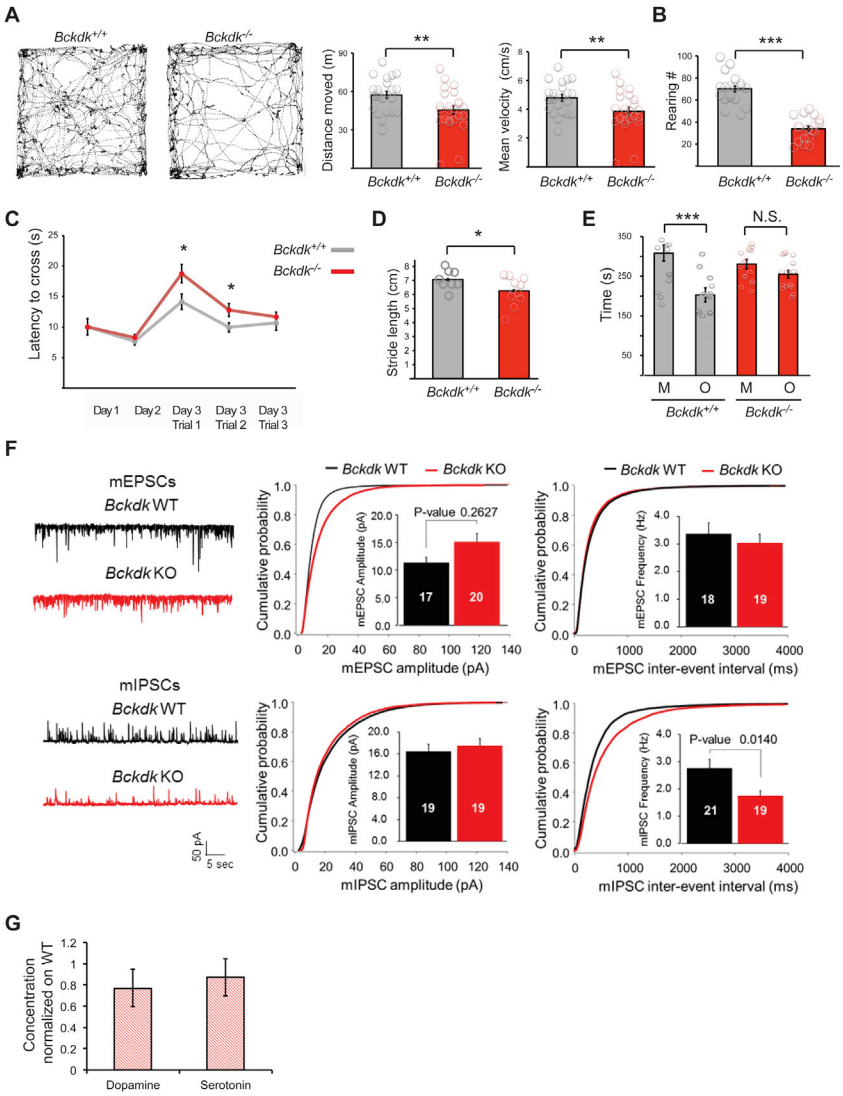

Figure S5. Phenotypic Characterization of *Bckdk*$^{-/-}$ Animals, Related to Figure 4

(A) Representative open field trajectories (left) and quantification of the total distance moved (middle) and the velocity during exploration (right); **p < 0.01 (means ± SEM; n = 25 mice per genotype; circles indicate individual values).

(B) Comparison of the number of rearings (anxiogenic forms of vertical exploration) of the two genotypes during the open field test, pointing out deficiencies in the mutants; ***p < 0.001 (means ± SEM; n = 18 mice per genotype; circles indicate individual values).

(C) Performance on the walking beam throughout the training days (Day1, Day2) and the three trials on the test day (Day3), showing elevated latency to cross the beam in the mutants; *p < 0.05 (means ± SEM; n = 23 mice per genotype).

(D) Stride length quantifications in the gait test reveal locomotor deficiencies in *Bckdk*$^{-/-}$ mice; *p < 0.05 (means ± SEM; n = 20 mice per genotype; circles indicate individual values).

(E) Bar graph quantifications of the number of contacts with the caged mouse (M) or with the caged object (O) in the three-chamber sociability test, revealing abnormal social interaction pattern in the mutant mice (mutants show no preference for the M over O, as opposed to controls); ***p < 0.001, N.S., not significant (means ± SEM; n = 16 mice per genotype; circles indicate individual values).

(F) Left: Representative mEPSC (top) and mIPSC (bottom) recordings from control *Bckdk*$^{+/+}$ (black) and *Bckdk*$^{-/-}$ (red) somatosensory cortex layers 2-3 pyramidal neurons; Right: Cumulative probability distributions of peak amplitudes and interevent intervals of mEPSC (top) and mIPSC (bottom) in the two genotypes. Insets: quantifications of mean amplitudes and mean frequencies of the corresponding currents. The significant reduction in mIPSC mean frequency detected in the mutants versus controls is indicated as absolute P value: *p < 0.05 (means ± SEM; n > 3 animals/genotype; number of recorded cells is noted on each column).

(G) Normal brain neurotransmitter levels in brain lysates of *Bckdk*$^{-/-}$ mice. Neurotransmitter levels were quantified by HPLC and normalized on protein concentration and on control littermate (*Bckdk*$^{+/+}$) levels; N.S., not significant (means ± SEM; n = 4 mice per genotype).

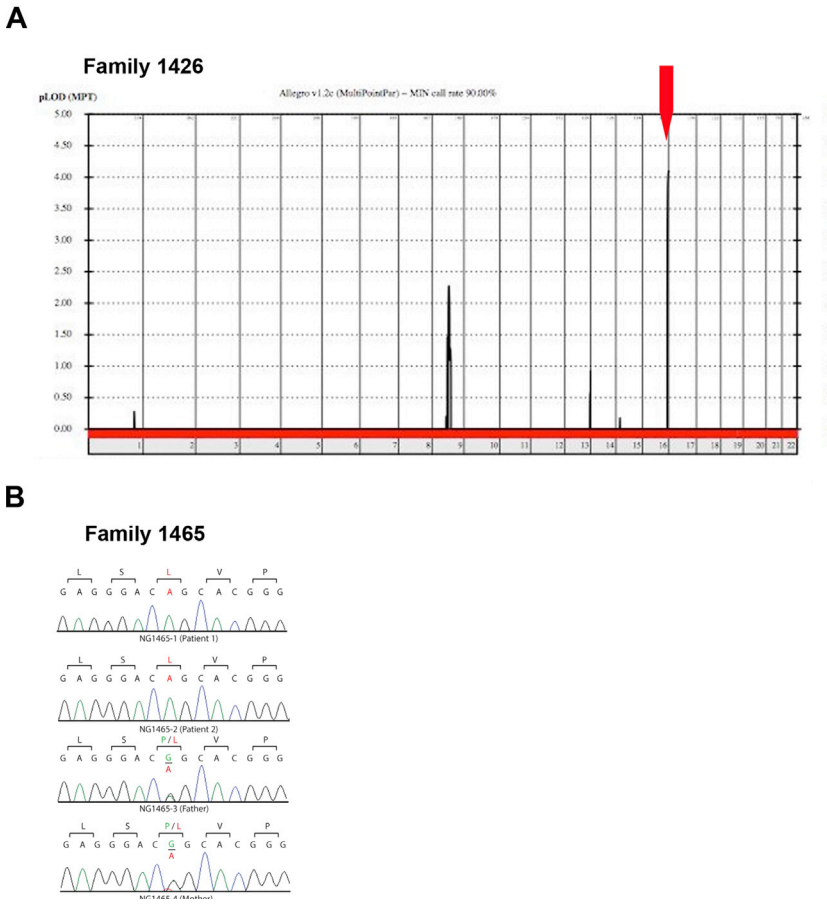

Figure S6. Genotyping Information of Family 1426 and 1465, Related to Figure 5

(A) Homozygosity map for Family 1426. Blocks of homozygosity are depicted as peaks. The red arrow indicates the interval that includes *SLC7A5*.

(B) Sequence chromatograms of all members of Family 1465 including the affected siblings and the carrier parents.

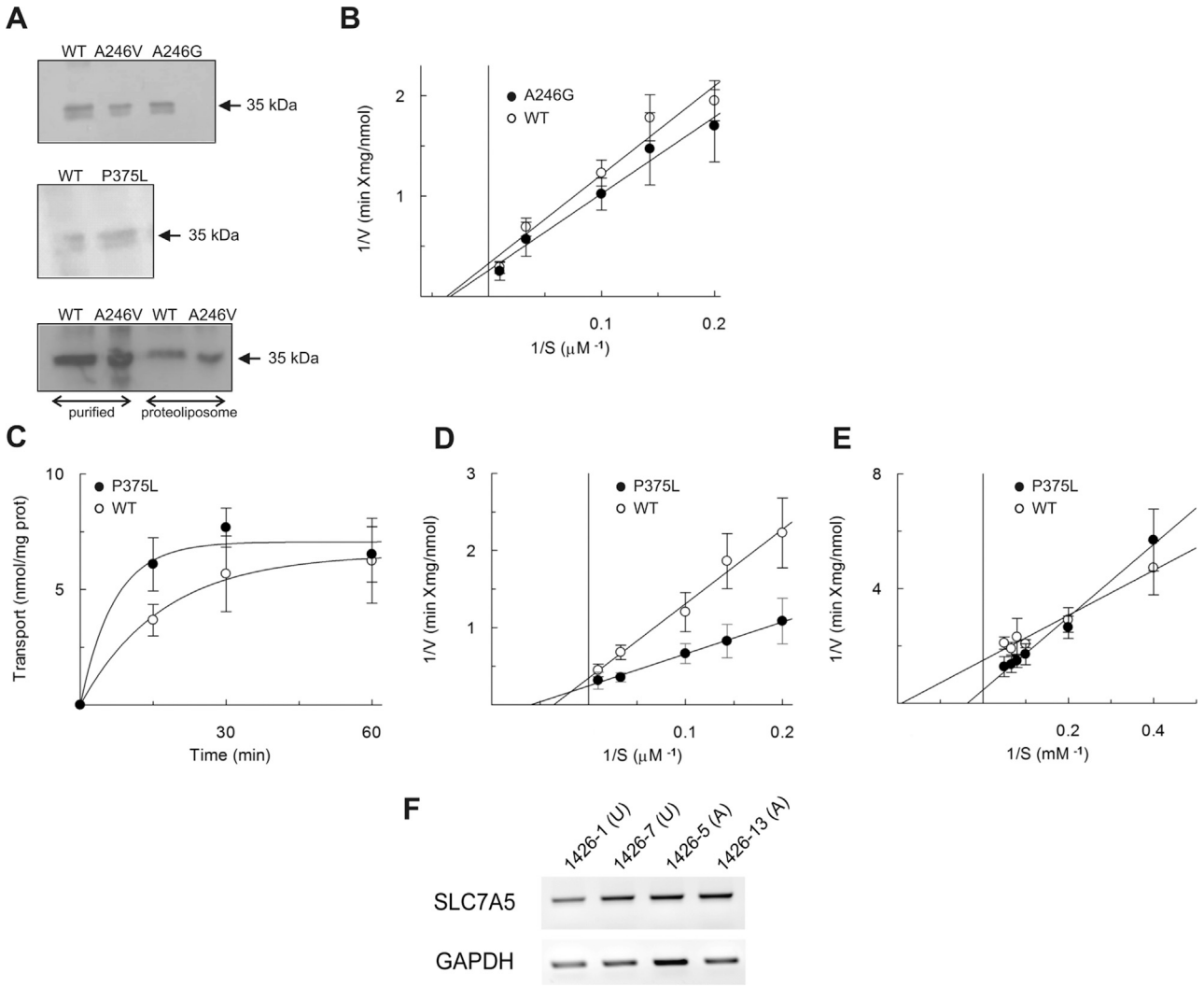

Figure S7. Characterization of SLC7A5-A246V, SLC7A5-A246G, and SLC7A5-P375L Mutants, Related to Figure 6

(A) Western blot analysis of the indicated SLC7A5 mutants in comparison with the WT protein reconstituted in proteoliposomes (top and middle panels). To evaluate the efficiency of reconstituted SLC7A5, proteoliposomes reconstituted with WT or SLC7A5 A246V were separated from liposomes (not containing reconstituted protein) by ultracentrifugation; blots of reconstituted proteins (proteoliposome) and of the purified protein before reconstitution (purified) are included in the bottom panel.

(B) SLC7A5-WT and SLC7A5-A246G-mediated transport rate (upon reconstitution in proteoliposomes) is dependent on external His concentration showing similar patterns for the two proteins. [^{3}H]-His was added at the indicated concentration to proteoliposomes containing 10 mM His, and transport stopped after 10 min (i.e., within the initial linear range of the time course). Data were fitted according to Lineweaver–Burk plot as reciprocal transport rate versus reciprocal His concentration (means ± SD; n = 3 independent experiments).

(C) Time-course of the transport mediated by SLC7A5-WT and P375L reconstituted in proteoliposomes, showing that the P375L mutant protein is functional. Transport was started by adding 5 μM [^{3}H]His at time zero to proteoliposomes containing 10 mM His reconstituted with WT- or P375L- SLC7A5 and stopped at the indicated times as described in the Experimental Procedure (means ± SD; n = 5 independent experiments).

(D) Rate of SLC7A5-mediated transport dependent on external His concentration. Transport rate was measured adding [^{3}H]His at the indicated concentration to proteoliposomes containing 10 mM His reconstituted with WT- or P375L-SLC7A5 protein. Transport was stopped after 10 min, i.e., within the initial linear range of the time course. Data were fitted according to Lineweaver–Burk plot as reciprocal transport rate versus reciprocal His concentration. (Means ± SD; n = 3 independent experiments).

(E) Rate of SLC7A5-mediated transport dependent on internal His concentration. Transport rate was measured adding 50 μM [^{3}H]His to proteoliposomes, containing the indicated His concentrations, reconstituted with WT- or P375L- SLC7A5 protein. Transport was stopped after 10 min, i.e., within the initial linear range of the time course. Data were fitted according to Lineweaver-Burk (or Michaelis-Menten) plot as reciprocal transport rate versus reciprocal His concentration. (Means ± SD; n = 3 independent experiments).

(F) Representative immunoblot showing *SLC7A5* transcript expression in human dermal fibroblasts; expression level is not affected by the A246V missense mutation (n = 3 independent experiments).